Received: 27 June 2022 | Revised: 13 June 2023 | Accepted: 14 June 2023

DOI: 10.1111/bre.12798

RESEARCH ARTICLE

Basin Research | IAS EAGE | WILEY

Pleistocene river diversions caused by large landslides in the western Pyrenees (Oria River drainage basin, N Spain)

V. Iribar | **B. Ábalos**

Departamento de Geología, Universidad del País Vasco UPV/EHU, Bilbao, Spain

Correspondence
V. Iribar, Departamento de Geología, Universidad del País Vasco UPV/EHU, P.O.Box 644, E-48080 Bilbao, Spain.
Email: vicente.iribar@ehu.eus

Funding information
UPV/EHU (GIU20/010)

Abstract

River-blocking landslides exert a deep impact on mountain range landscapes and the organization of catchments. A blocked river diverted to another watershed modifies both original and transferred drainage networks both up- and downstream. Using western Pyrenees examples, a geological and geomorphic framework with diagnostic criteria to detect river diversion by landslides is presented, including the identification of elbows of diversion, eroded divides, beheaded underfit rivers, diverted overfit rivers, reversed river segments and the landslides at fault. Some landslides caused the formation of lakes that overflowed upstream at catchment divide segments with elevations lower than those of blocking landslide tops. Unravelling the presence of fan deltas at distinct sites/elevations of palaeolake shores contributed as well to identification of river damming and later diversion episodes. Reconstruction of the sedimentary organization of river palaeovalleys and of their associated fluvial terraces and palaeoriver channels (some currently submerged by the Cantabrian Sea), along with the reconstruction of river profiles, analysis of bedrock and morphology of watershed divides, identify seven river diversions caused by landslides and 14 additional slides that variably constrained river basin dynamics in the area studied. The diverting slides have current areas between 0.06 and 12.3 km^2 (thus including giant examples), thicknesses up to 300 m and translational–rotational rupture surfaces usually with low dip angles (3.5–12.3°). A combination of relative dating methods and published absolute ages suggests that diversion events occurred during the Quaternary. This study shows that river diversion by landslides can be significant in mountainous areas of moderate relief.

KEYWORDS

landslides, palaeovalleys, Quaternary, river diversion, western Pyrenees

1 | INTRODUCTION

River diversion (the capture and redirection of a given basin's drainage to an adjacent watershed) is a relatively common and consequential geological event (Bishop, 1995). Firstly, diversion modifies the geomorphology, the balance of erosion/transport/sedimentation and the ecology of river basins. Second, river diversion is usually the result of some rapid geological process (Twidale, 2004). The most direct process is fluvial capture (or piracy) by headward erosion of another river flowing at a lower level (Davis, 1890) and can be caused by other mechanisms such as tectonic tilting, faulting, anticline growth or diapiric uplift. Other processes causing diversion are related to valley damming by ice, volcanism or landslides, which cause the rupture of the catchment divide by overflow of the dammed lake. In high-mountain and arid areas with good geological exposure, the cause of diversion may be obvious. However, in heavily vegetated or urban areas, it may be difficult to identify diversion and its cause, which may be further obscured because of weathering, hillslope overprinting, erosion processes and sea-level change (e.g., long-range flooding). In these cases, identification of river diversion events can direct the research to reveal the obscured geological processes that caused it.

Recognizable morphological criteria in drainage networks affected by diversion include: elbows of capture, barbed drainage, wind gaps, transverse drainage and knickpoints; these features are collectively referred to as anomalous drainage (Twidale, 2004). Chi maps of adjacent basins are also used to detect river diversion (Guerit et al., 2018; Willett et al., 2014). When river diversion occurs, one basin increases its surface area while that of the other decreases. Therefore, because the morphological features on river basins are related to its area, two basins with anomalous drainage patterns are to be expected. Geological criteria involve the materials related to palaeodrainage alterations, which may form terraces, valley floor sediment infillings, etc. (Bishop, 1995). Since sediment grain size distribution, slope geometry (Bhattacharya et al., 2016), dimensions of palaeochannels (Gibling, 2006) and the size of palaeovalleys (Wang et al., 2019) are related to river basin area, anomalies in the relationship between these features and the basin area may be indicative of river diversion, too. By combining geomorphic and geological criteria, Douglass et al. (2009) distinguished the transverse drainage (diversion) mechanisms called antecedence, superimposition, capture and overflow.

Obstruction of rivers by landslide dams is common in steep mountainous areas with deep narrow valleys. The blockage forms lakes upstream that after eventual overflowing can breach and progressively destroy the dams (Costa & Schuster, 1988). The landslide toe can laterally displace the course of a river (Korup, 2006; Korup et al., 2007) or create epigenetic gorges (Ouimet et al., 2008). For diversion to occur, the height (relief) of the landslide dam must be higher than the lowest drainage divide elevation (height above sea level) upstream, and diversion would occur in this site when the lake is filled up to that elevation. Landslide dams affecting the drainage divide are considered rare and difficult to track due to low preservation potential (Fan et al., 2020; Hermanns, Hewitt, et al., 2011). Lake Crescent (Logan & Schuster, 1991) and Lake Agrio (Hermanns, Folguera, et al., 2011) are the only documented cases to our knowledge. Additionally, a dammed lake of non-tectonic origin is ephemeral on geological time scales (Garcia-Castellanos, 2006).

This article shows that river diversion by landslides can be significant in mountainous areas of moderate relief. It is presented firstly a geological and geomorphic framework with diagnostic criteria to detect river diversion by a combination of the formation of lakes by landslide damming, river diversion by overflow, divide erosion and, finally, lake draining. Then, the geomorphology and sedimentology of fluvial, coastal and incised palaeovalleys in the Oria River and neighbouring small catchments of the western Pyrenees are studied. The analysis permitted identification of several river diversions caused by landslides and of additional slides that variably constrained the regional river basin dynamics during the Quaternary.

2 | MORPHOLOGICAL FEATURES OF RIVER DIVERSION

A working scheme is presented here that uses characteristic geomorphic features to identify: the formation of lakes by landslide damming, river diversion by overflow and divide erosion and lake draining (Figure 1). If a landslide creates a natural dam in one of two adjacent river basins (Figure 1a), a lake will form. If the elevation of the dam (h_L) is greater than the elevation of the divide (h_D) at a given location, when the lake level attains h_D, overflow will begin to erode the divide (Figure 1b) there. After complete erosion of the divide and drainage of the lake, a new drainage pattern will result with several diagnostic geomorphic features (Figure 1c) as those described below.

2.1 | Elbow of diversion

This is the point where a river abandons its previous course and is directed towards the ancient divide. It is recognized by an abrupt change in the river channel direction. This feature is similar to the elbow of capture by Bishop (1995) and Ma et al. (2023).

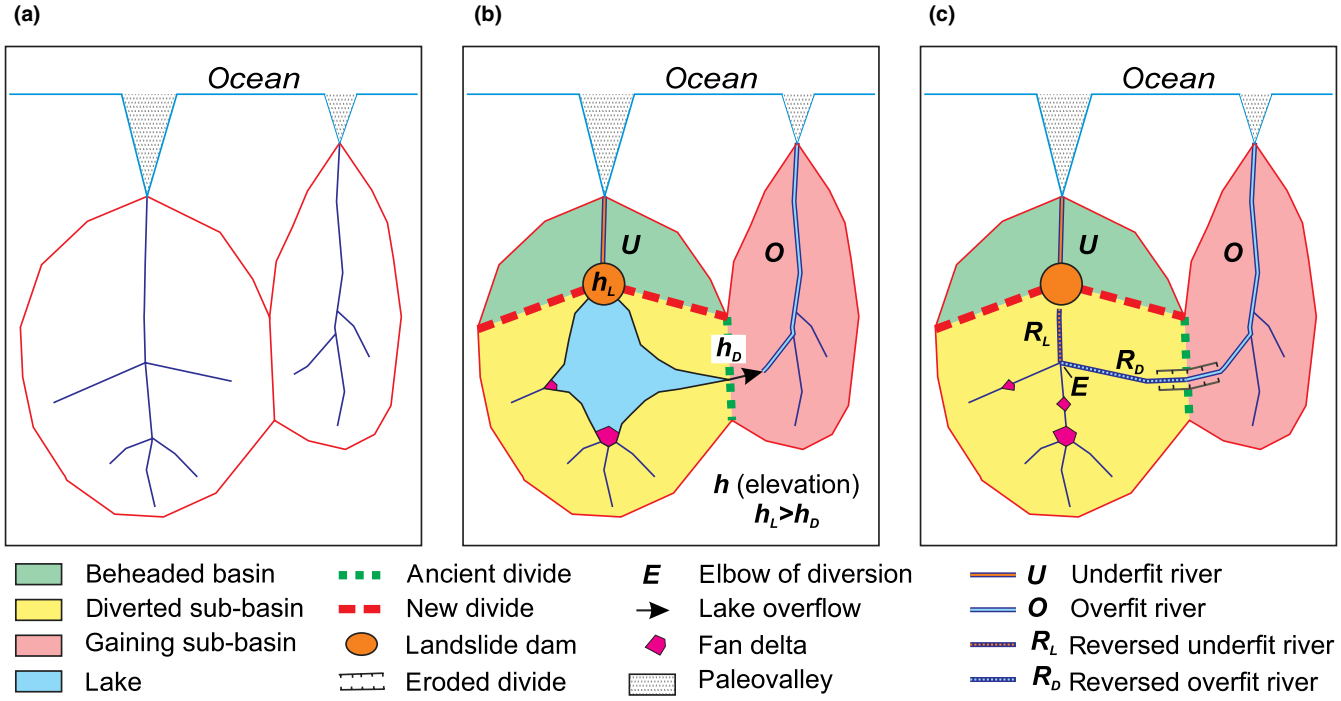

FIGURE 1 Sketches showing the geomorphic features expected after a river is dammed and diverted by a landslide. (a) Pre-landslide geography. (b) Formation of a lake by landslide damming and eventual overflow. (c) Reconfiguration of the drainage network and catchment boundaries after erosion of the divide.

2.2 | Eroded divide

This is the point where a dammed lake overflows a former catchment divide. It can evolve into a gorge in hard rock terrains (Anton et al., 2015), or conform to a narrow valley in areas dominated by soft rocks. When considering the geological structure, it can also be referred to as transverse drainage (Douglass et al., 2009).

2.3 | Beheaded underfit river

This is the river formed downstream of a blocking landslide as the main river loses its headwaters and becomes underfit. Underfit rivers bear a much smaller watercourse than that reasonably expected in view of the size of their valleys. They are also expected to exhibit small meander wavelengths relative to their alluvial valley dimension (Davis, 1913; Dury, 1964).

2.4 | Diverted overfit river

This is the river segment of a neighbour catchment that seized the water flow of the diverted river downstream of the eroded divide. It usually appears as a river with a flow too big for the valley through which it circulates. An overfit state can thus be inferred by comparing the rations of water flow and valley width/dimensions in neighbouring rivers.

2.5 | Reversed underfit river (R_L in Figure 1c)

This is the segment of the original river network situated between the blocking landslide and the elbow of diversion. The flow of the ancient river in this segment is reversed (and reduced) after diversion and the ensuing valley is usually (and counter-intuitively) narrower downstream. This river segment will have an underfit state.

2.6 | Reversed overfit river (R_D)

This is the segment of the original river situated between the elbow of diversion and the eroded divide. This is a former tributary channel that underwent a flow reversal and as a result can associate a valley narrower downstream, too. The ancient tributary will turn into an overfit state.

2.7 | Fan deltas

These are a variety of alluvial fans formed at the point where a river enters a lake and spills its sediment load.

In the case of landslide-dammed lakes, fan deltas are expected to form on the new mouths of both the main river channel and the major tributaries after a given lake-level stabilization. Fan deltas bear sub-horizontal top surfaces (topsets) and inclined frontal prograding parts (foresets), the knickpoint separating them being a good approximation to lake water palaeosurface. The elevation of the highest fan delta preserved is constrained (limited) by the lowest elevation of the original river basin divide at the site of the new divide. As the latter is progressively eroded, other fan deltas can develop at lower elevations, the earlier ones being variably preserved, dissected or even dug out (Eddey et al., 2022; Link et al., 2014).

2.8 | Landslide dam

This is a landslide structure that obstructs or blocks a former river course. It is usually formed/emplaced at a rate faster than the river erosion potential and thus becomes a barrier to water flow. As a result, a lake forms upstream that will grow until overflowing the new catchment either at the landslide top (initiating there the dam removal) or at a basin divide point with a lower elevation (Figure 1b,c).

Contrary to fluvial capture landforms, in the scheme described above, dry valley segments or 'wind gaps' of the beheaded stream are lacking downstream of the elbow of diversion. Also, in this scheme, the presence of the geomorphic features described can be supported by means of sedimentological characteristics present in the catchment areas. Changes in basin dimensions can influence sediment flow and transport (Bhattacharya et al., 2016). Therefore, assessment of coarse sediment size and thickness relative to basin size can help identify a river's reach as underfit.

Fluvial terraces and fan deltas are in principle rather different geological features, geomorphologically, sedimentologically and genetically. However, coarse-grained terrigenous deposits with gently dipping top surfaces next to a river might be classified either as terraces or as eroded fan deltas. Terraces typically form in basins that have reached a critical size (about 60 km^2; García, 2006). On their part, alluvial plains form in river reaches with slopes less than 0.8% (Fryirs & Brierley, 2013). Keeping this in mind, sub-horizontal deposits located adjacent to rivers with small basins and steep slopes are less likely to represent terraces or alluvial plains than fan delta topsets. In narrow valleys of larger rivers, the existence of dammed lakes could facilitate the construction of laterally confined fan deltas (Nemec & Steel, 1988). These occupy the width of valleys and have a greater potential for progradation and aggradation than unconfined fan deltas. When dissected, the remains of confined fan deltas can resemble fluvial terraces (Zhang et al., 2016).

3 | PHYSICAL GEOLOGY CONTEXT AND PREVIOUS WORK

The Oria River basin is located on the coastal inner corner of the Bay of Biscay (northern Spain; Figure 2a). This region connects the Pyrenees (to the E) and the Cantabrian Mountains (to the W). The study area comprises, in addition to the Oria basin, the closely related catchments of the Urumea, Oiartzun, Iñurritza and Añorga Rivers (Figure 2b; Table 1). Lower and middle parts of the Oria River basin can be distinguished, separated by the Bazkardo gorge (Figure 3). The middle Oria sub-basin (to the south) includes the Leitzaran and Zelai tributary river watersheds. In the area shown in Figure 3, the average terrain slope is 0.22, and the mean local relief measured within a 5 km circular window is ca. 300 m at the northern (lower Oria) sub-basin and ca. 600 m at the southern one.

Current rainfall in the Oria River basin is 1.3 m/year and the average annual runoff is 26 m^3/s. Its annual suspended sediment discharge to the ocean has been estimated at 173 t/km^2/year (Zabaleta et al., 2016), the sediment delivery ratio with respect to catchment erosion being 59% of 217 t/km^2/year. These figures can be correlated with a catchment yearly homogeneous removal of 0.09 mm of surface rocks. By contrast, the Urumea catchment 2.5 m/year rainfall in an area ca. 1/3 as small as Oria's basin dimension results in a suspended sediment discharge to the ocean of only 10 t/km^2/year (Zabaleta et al., 2016).

Geologically, the area forms part of the 'Basque Arc' of the 'Basque-Cantabrian Basin'. Barnolas and Pujalte (2004) and Ábalos (2016) reviewed the details of this realm's organization and terminology in the geological literature. The 'Basque Arc' domain experienced extensive faulting and high subsidence rates during the Cretaceous, and was inverted during Tertiary compression related to the Alpine Orogeny (Gómez et al., 2002). Currently, it is considered a hyper-extended rifted domain with a thinned lower continental crust and local exhumed subcontinental mantle (Pedrera et al., 2017, 2021; Teixell et al., 2018, and references therein). Cuevas et al. (1999), Bodego and Agirrezabala (2013) and Ábalos (2016) reviewed the stratigraphic, structural and metamorphic details of the Basque Arc rocks, cropping out widely in the Oria River basin (Figure 2b). Mechanically harder lower Triassic red sandstones and Aptian limestones constrain the highest elevations in the area, whereas softer siltstones, lutites, marls and flysch successions of various ages form mountain hillslopes and valleys. Among the

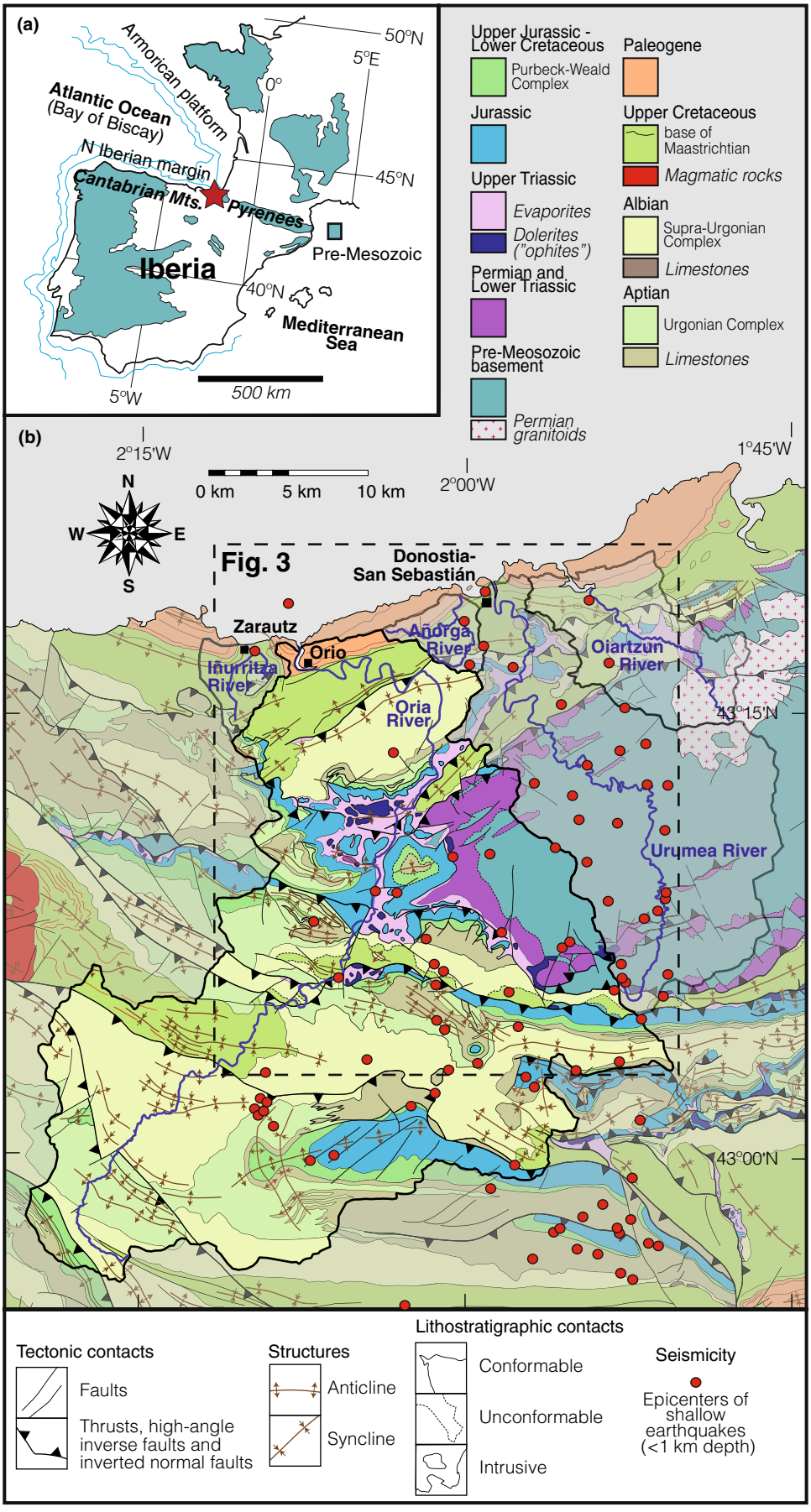

FIGURE 2 Geological map of the area studied (modified after Ábalos, 2016). See text for further comments.

TABLE 1 Dimensions of geomorphic features of fluvial origin.

	Oria	Urumea	Oiartzun	Inurritza	Añorga	Leitzaran	Zelai
Basin area (km^2)	874	274	86	23	18	124	34
Alluvial plains; total area (km^2)	26.0	9.3	3.5	3.1	1.2	1.4	1.4
Scattered alluvial plains area (km^2)	0.56	0.34	0.06	0	0.15	1.33	0.77
River terraces (km^2)	1.8	0.4	0.2	-	-	-	-
Palaeovalley area[a] (km^2)	4.1	6.8	2.20 (land) 0.34 (sea)	2.3	0.9		
Palaeovalley length (km)	12.0	12.5	6.5	2.0 LB; 2.8 RB	2.5 LB; 2.0 RB		
Palaeovalley max. depth at the coast (m)	−42.7	−42.6	−25.0	−48.4	−36.0		
Palaeovalley mean slope (%)	0.44	0.40	0.47	3.87 LB, 0.75 RB	0.44		
Palaeovalley basal gravel bed thickness at the coast (m)	4.8	5.8	3.5	1.5 LB 0 RB	1.0?		
Submerged delta surface (km^2)	8.5	1.0	0.1	10.0	Confluence with		
Submerged delta max. depth (m)	−55	−17	−22	−55	Urumea River		
Palaeoriver channel(s) depth: min; max	−55; −70	−18;-40, W −18; −70, C −18; −40, E	−22; −30	-	-		
Palaeoriver channel(s) width (m)	150–200	60–70, W 150–250, C 60–70, E	30	-	-		

Abbreviations: C, central; E, eastern; LB, left branch; RB, right branch; W, western.

[a]Palaeovalleys are completely filled except for the Oiartzun valley.

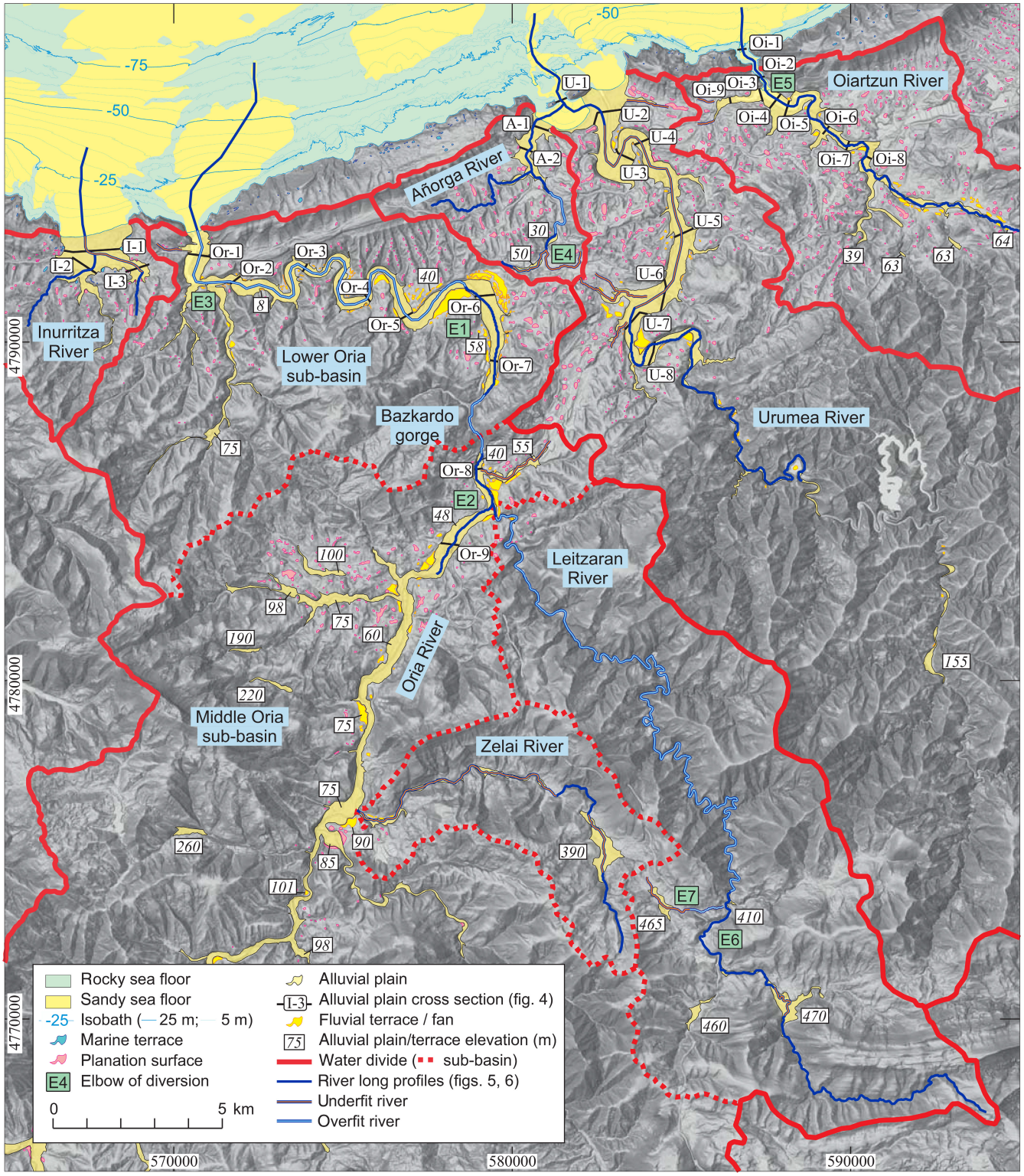

FIGURE 3 Shaded relief geomorphological map of the area studied after 5-m-resolution digital elevation model of the Spanish Instituto Geográfico Nacional (www.ign.es). UTM zone 30 coordinates, ETRS89 datum. The framed labels (U-1, etc.) mark the positions of stratigraphic cross-sections shown in Figure 4 for (from W to E) the Iñuritza (I-1 to I-3), Oria (Or-1 to Or-9), Añorga (A-1 and A-2), Urumea (U-1 to U-8) and Oiartzun (Oi-1 to Oi-9) Rivers.

soft rocks, upper Triassic evaporites are remarkable because, on one hand, they exerted control during Mesozoic sedimentation and Cenozoic (Alpine) tectonic inversion and, on the other hand, they constrained the current courses of significant segments of the Oria and Urumea Rivers (Figure 2b).

To date, the area can be considered tectonically active, affected by several low-magnitude earthquakes (Dumont et al., 2015; Ruiz et al., 2006). A survey in the Spanish Instituto Geográfico Nacional database (https://www.ign.es/web/ign/portal/sis-catalogo-terremotos/) of the earthquakes recorded between January 1, 1900, and June 7, 2022, in the area bounded by latitudes 42°55′ and 43°20′N and longitudes 1°50′ and 2°10′W yielded 251 events. From them, 8.9% were of magnitude <1, 60.5% between 1 and 2, 21.4% between 2 and 3 and only 7.7% exceeded magnitude 3 (with only one reaching M 3.9). Nearly 35.0% of the seismic events had shallow hypocentres of <0.2 km (Figure 2b), bearing a magnitude (M) distribution of 18.0% <1, 65.1% between 1 and 2, 10.5% between 2 and 3 and five M >3 events.

The Cantabrian Mountains experienced Quaternary rock uplift at estimated rates ranging between 0.07 and 0.15 mm/year in their central sector (Alvarez-Marrón et al., 2008), with elevation intensity increasing to the E during the last 1–2 Ma. The uplift follows 8–10 km of Alpine exhumation related to the ca. 115 km orogenic shortening registered in the W-Pyrenean sector of the North Iberian convergent margin (DeFelipe et al., 2018, 2019; Teixell et al., 2018) due to indentation of the European and Iberian lithospheres.

Exhumation average rates (mostly due to erosional unroofing) have been estimated in the range 0.13–0.24 mm/year after Oligocene times, with tectonically driven fast initial episodes (0.77 ± 0.08 mm/year) between 45 and 35 Ma (DeFelipe et al., 2019). The Oligocene–Miocene transition ca. 20 Ma ago appears to mark the turn from Alpine convergence to incision of fluvial networks as principal exhumation cause. The post-Oligocene exhumation rate can be considered the upper limit to Quaternary rock uplift rate; both exceed slightly current catchment erosional removal rate (0.09 mm/year).

Ríos (1948) and Santana (1966a) anticipated the likely occurrence of river diversion in this area. The first author related diversion to diapiric activity, attending to the close relationship between Triassic evaporite outcrop distribution and anomalous segments of the river's current course (Figure 2b). The second author studied and discussed further this issue, eventually ruling out the possible diversion of the Oria River since its original mouth would have been displaced 10 km W from San Sebastián to its current location in the Orio estuary.

4 | METHODS

4.1 | Mapping of fluvial, coastal and sea bottom geomorphology

Fluvial and coastal geomorphic features were mapped using LiDAR-based digital elevation models (DEM) of 1, 5 and 25 m resolution (b5m.gipuzkoa.eus: 2008 flight; www.ign.es). Surfaces with inclinations <10° in the 5-m-resolution DEM were identified as possible coastal and fluvial terraces, following guidelines proposed by Demoulin et al. (2007). They were also used in the Oiartzun basin by del Val et al. (2015). The 1-m-resolution DEM was also used to look for detailed geomorphic features, whereas the 25 m DEM was employed for construction of longitudinal river profiles and measurement of river sinuosity. Low-slope terrains are scarce in the area and, thus, were progressively occupied by cities and roads, hereby concealing the geology and geomorphology underneath. In order to counteract this drawback, ancient topographic maps and aerial photographs were also used for the mapping work, including those of the Cuerpo de Ingenieros Militares (1852), 1966–1985 1:5.000 scale maps, and a 1954 aerial photography survey at 1:12.000 scale. These tools are hosted by local and regional administration institutions (e.g., b5m.gipuzkoa.eus).

Bathymetry data (with 1 m contour interval) and sediment-type data from the coastal seabed up to depths of 100 m were collected from regional administration databases (ftp.geo.euskadi.net/cartografia/). In the case of the mouth of the Oiartzun River, it was dredged from 1870 to 1985 to build a port. The available technical information together with complementary old and new maps of the port were used, too, including Tofiño de San Miguel (1788), the (1909) 'Plano del Puerto de Pasajes' at 1:5.000 scale (Sociedad General del Puerto de Pasajes) and the (2002) bathymetric map n. 3911 at 1:5.000 scale (Spanish Hydrographic Institute). In the coastal area of the Urumea River, detailed data reports from recent sedimentological dredge and seismic surveys were scrutinized (AZTI, 2015; ESGEMAR, 2015; OCSA, 2015).

4.2 | Stratigraphy and sedimentology of alluvial fills, incised palaeovalleys and fluvial terraces

Around 750 borehole logs drilled in the alluvial plains and some terraces for geotechnical and hydrogeological surveying were examined. These contain log information on recent sediment thickness and lithology and, in some cases, are publicly available (www.gipuzkoa.eus/es/web/obrahidraulikoak/mapas/catas-y-sondeos). Sediment characteristics were interpreted as facies types using the criteria of Miall (2014) for fluvial facies and Dalrymple et al. (2012) for estuarine facies. The interpretation was also based on facies recognized in boreholes (Monge-Ganuzas et al., 2019), superficial characteristics of other estuaries of the Bay of Biscay (Flor-Blanco et al., 2015) and observations made on terraces with accessible outcrops. Borehole information was employed for constructing 31

transverse cross-sections of the alluvial fills (Figure 4). All this was completed with published chronological information collected from available absolute dating determinations in the area.

Combining the topography of bedrock reaches, alluvial plain fills, palaeovalleys, submerged palaeoriver channels, river terraces and fan deltas, geological profiles (Figure 5) were reconstructed along the thalwegs of five coastal river basins (Figure 3). In the case of the Leitzaran and Zelai Rivers, longitudinal profiles include bedrock lithology data (Figure 6). In the Leitzaran River, its sinuosity (following Johnson, 2016) was determined as the ratio between along-path distance of the stream and straight-line distance between two points, measured every 50 m at lengths ranging from 50 to 1.000 m (the highest sinuosity measured for each point being picked).

4.3 | River diversion and palaeolandslide recognition

River catchment geometrical features were analysed to unravel diversion events following the ideas synthesized in Figure 1. First, we considered river reaches' planforms (Willett et al., 2014), profiles and sedimentary characteristics in order to identify and classify reaches as underfit or overfit and locate elbows of diversion (Figure 3). This led us to hypothesize where potential diversion sites might be located. For each suspected diversion, two river-long profiles were constructed: one intended to connect former upstream and downstream reaches (so far separated by a landslide) and a second profile done on purpose to restore former divides that currently are recognizable as gorges (Figure 7). Sedimentological data were considered likewise in order to support or reject the feasibility of diversion events. Also, the location and elevation of fluvial terraces and fan deltas were examined to shed light on the existence of palaeolakes. Next, identification of palaeolandslides was explored after close inspection of the geology and geomorphology of the current catchment divides. Comparison of the elevations of landslide dams and fan deltas was considered a reinforcing issue. To this end, topographic data and geological map collections at 1:25.000 and 1:50.000 scales were analysed. The geological maps used are publicly available and hosted by regional and national Spanish institutions: 'Ente Vasco de la Energía' (EVE, 1:25.000 maps, https://www.eve.eus), Gobierno de Navarra (1:25.000 maps, https://geologia.navarra.es) and 'Instituto Geológico y Minero de España' (IGME, 1:50.000 maps, https://mapas.igme.es/Servicios/default.aspx). In some cases, local geological reports and published articles were also used.

5 | RESULTS

In the following sub-sections, the geomorphic characteristics and sedimentary facies of different features cited are described in detail. In the inland area, four gentle-slope geomorphic element types are identified: alluvial plain fills (associated with palaeovalleys), fluvial terraces/fans, marine terraces and estuarine terraces. Additionally, several river reaches have been classified as underfit or overfit. Below the current sea level, two types of seafloor surfaces are distinguished: bedrock outcrops and sediment-covered areas (see also Figure 3 and Table 1). Cross-sections of alluvial plains are shown in Figure 4, meanwhile longitudinal profiles of palaeovalleys and river thalwegs are shown in Figures 5 and 6.

5.1 | Alluvial plain fills and palaeovalleys

Alluvial plains in the Oria drainage basin extend continuously from the coast towards the headwater areas following the main trunk and major tributaries. Alluvial plains are absent, however, at the Bazkardo gorge (Figure 3). This is a transverse drainage excavated across hard lower Cretaceous limestones that currently forms a gorge separating the lower and middle Oria sub-basins.

The Oria River has the greatest extension of alluvial plains in the area studied (56 km^2; Table 1), which is ca. 3% of the catchment area. It is noteworthy, taking into account scaling catchment area relationships with other basin features, that the small Iñurritza River basin (23 km^2) exhibits the highest ratio between alluvial plain and catchment areas (13%). whereas the much larger Leitzaran River (124 km^2; Table 1) presents the lowest (1%). In several catchments, there exist dispersed alluvial sediment patches disconnected from the main (and largest) continuous alluvial plain edifices. Leitzaran and Zelai are the rivers that associate the maximum extent of those patches, in

FIGURE 4 Stratigraphic cross-sections of alluvial valley and palaeovalley infillings. All sections share the same horizontal scale and a vertical exaggeration x10. See Figure 3 for location of the sections in the different drainage networks. (a) Urumea River (cross-sections U-1 to U-8). (b) Oria River (Or-1 to Or-9). (c) Oiartzun River (Oi-1 to Oi-9). (d) Iñurritza River (I-1 to I-3). (e) Añorga River (A-1 and A-2). The left side of the sections corresponds to the left side of alluvial valleys (looking downstream). Section Or-1 adapted from Euroestudios (1971), Or-2 was completed after DFG (2006) and Oi-3 and Oi-4 after Valdés (1942).

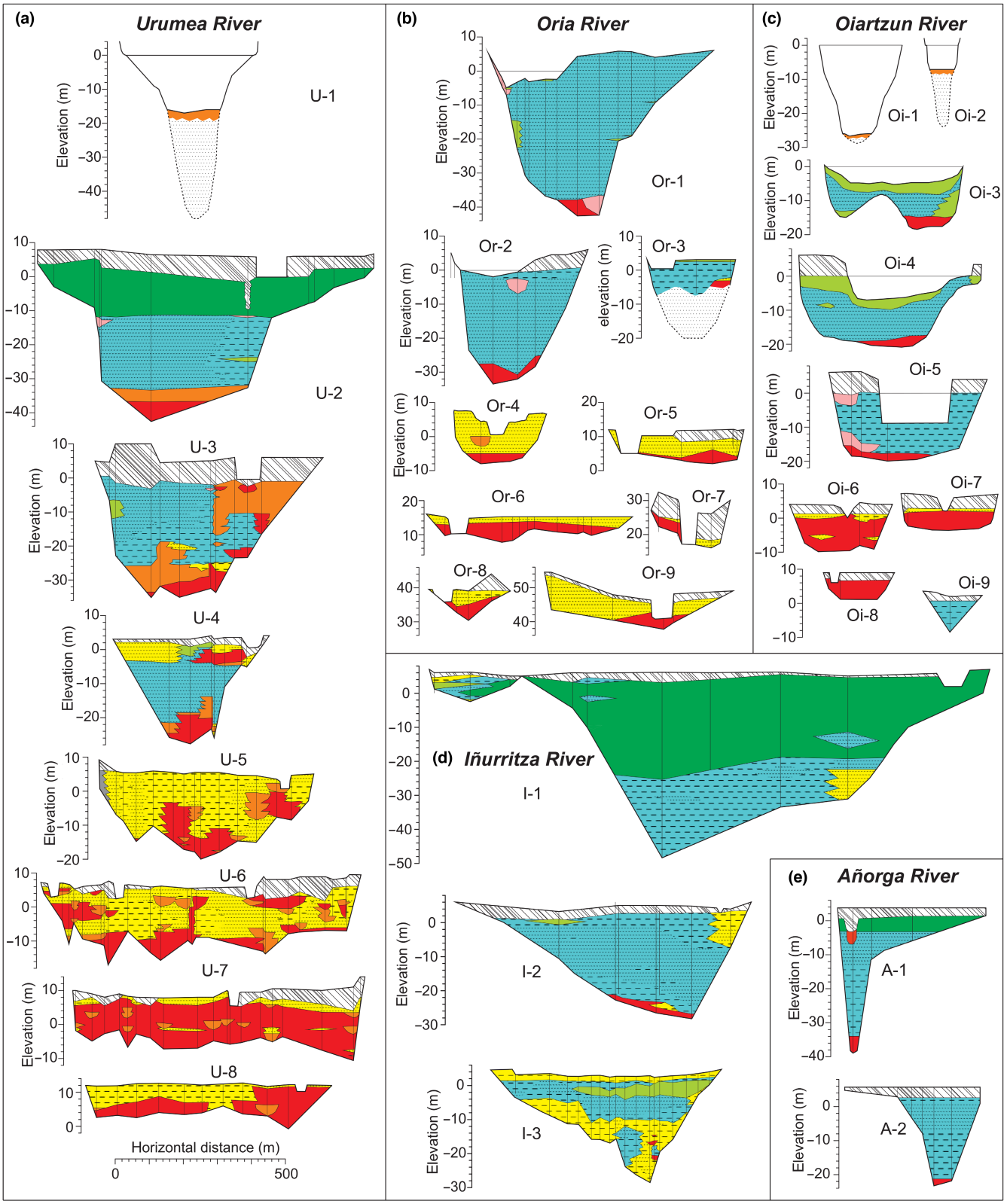

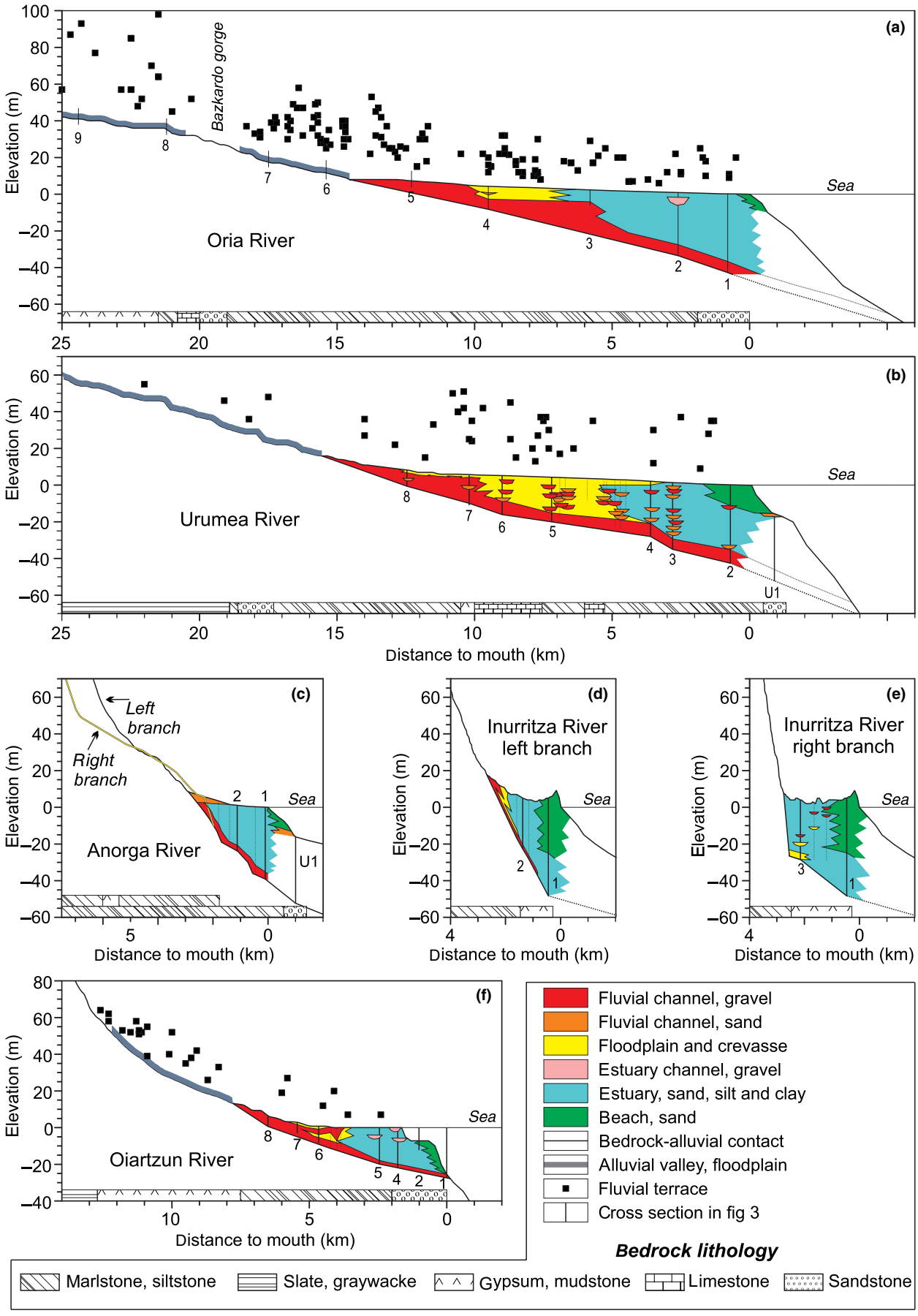

FIGURE 5 Longitudinal profiles of rivers and palaeovalleys in the coastal area. (a) Oria River. (b) Urumea River. (c) Añorga River. (d and e) Iñurritza River (left and right branches, respectively). (f) Oiartzun River. All sections share the same horizontal scale and a vertical exaggeration x10. Black small squares in (a, b and d) mark the positions and elevations of fluvial terraces identified along the river hillslopes.

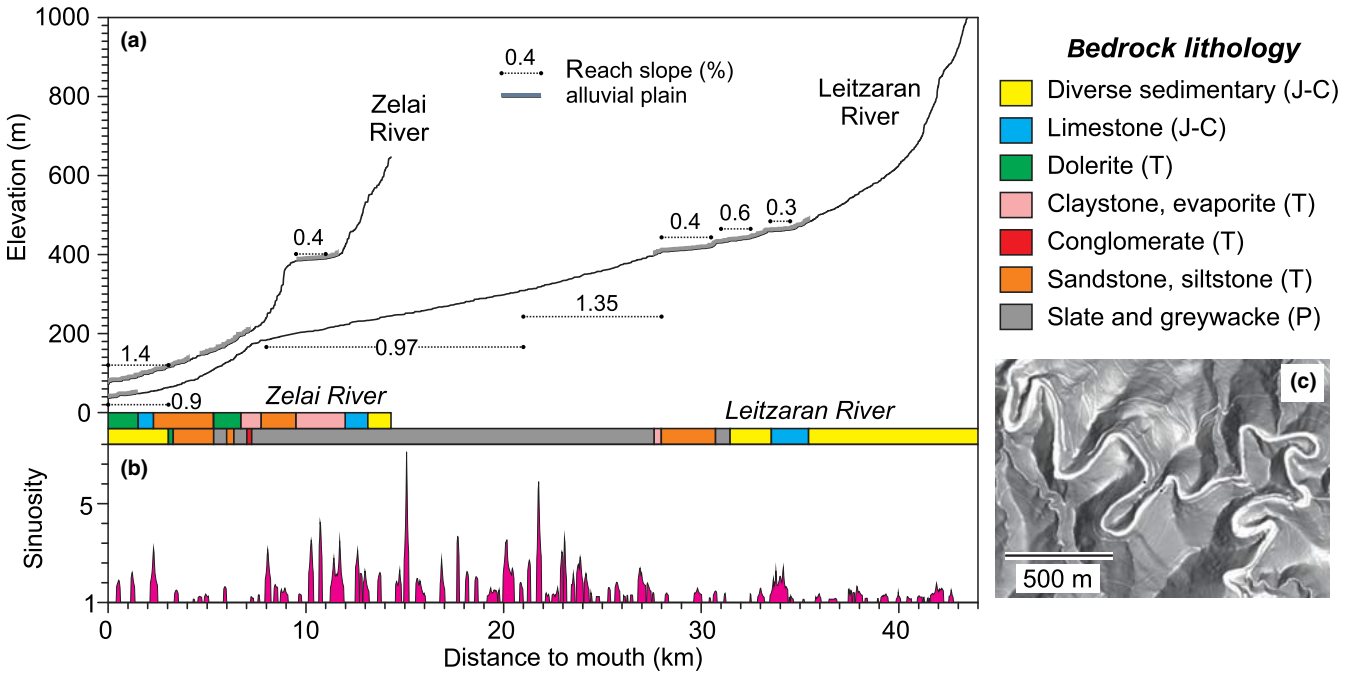

FIGURE 6 (a) Longitudinal profiles of the Leitzaran and Zelai rivers showing various low-slope segments and bedrock lithology along their courses (horizontal axis). Note the vertical exaggeration x20 with respect to the horizontal scale. (b) Sinuosity of the Leitzaran River (see text for further details). (c) Close view of the digital elevation model (see Figure 3) of the Leitzaran catchment area around the river segment located between 20.0 and 24.5 km from its confluence with the Oria River.

most cases at high elevations (Table 1). Occurrence of disconnected alluvial patches cannot be easily explained on lithological or structural grounds (with the exception of a karstic depression fill in the left Oria River wing).

Thickness of alluvial plain sediment accumulations varies from a few meters in the middle reaches of catchments up to 50 m in coastal palaeovalleys incised below the current sea level during previous glacioeustaic lowstands. The Urumea River associates a coastal alluvial plain and palaeovalley infill (>45 m thick) slightly larger (6.8 km^2) than the associated to the >3 times larger Oria rived catchment (Table 1; Figure 3). The chronostratigraphic ^{14}C age of the youngest coastal palaeovalley infillings is Holocene in most cases (see Table 2 and references therein). On their part, the Urumea and Iñurritza palaeovalley basal sediments yielded Late Pleistocene ages (25.3 to >43.5 ky; Table 2).

Six sediment facies and five sub-facies types were distinguished for representation in the cross-sections and longitudinal profiles of alluvial plain fills presented in Figures 4 and 5. They are described in the following sub-sections.

5.1.1 | Fluvial channel gravel facies

It consists of gravel with rounded clasts in a sandy terrigenous matrix. Clast grain sizes reach up to cobble and boulder granulometric classes (up to 50 cm in diameter). It is interpreted here that this facies originated in a high-energy sedimentary environment, likely related to braided rivers. In the coastal area, the maximum thickness of this facies is 5.8 m in the Urumea palaeovalley infill (Table 1), whereas it is almost absent in the Iñurritza palaeovalley. Subsurface log data present this facies usually in the lower part of palaeovalley infillings (Figures 4 and 5). Log correlations in alluvial plain apex zones show continuous, km-long and a few-m-thick coarse-grained terrigenous bodies that compose the principal facies type (Figure 5). Gravel body thickness is greatest inland from the current coastline. Additionally, the reconstructed geometry of this facies along the river flow direction presents frontal progradating terminations. These might be associated with fan-delta foresets and related facies changes. Towards the coastline, this facies can also form small lens-like bodies (channel infillings) within finer-grained sediments.

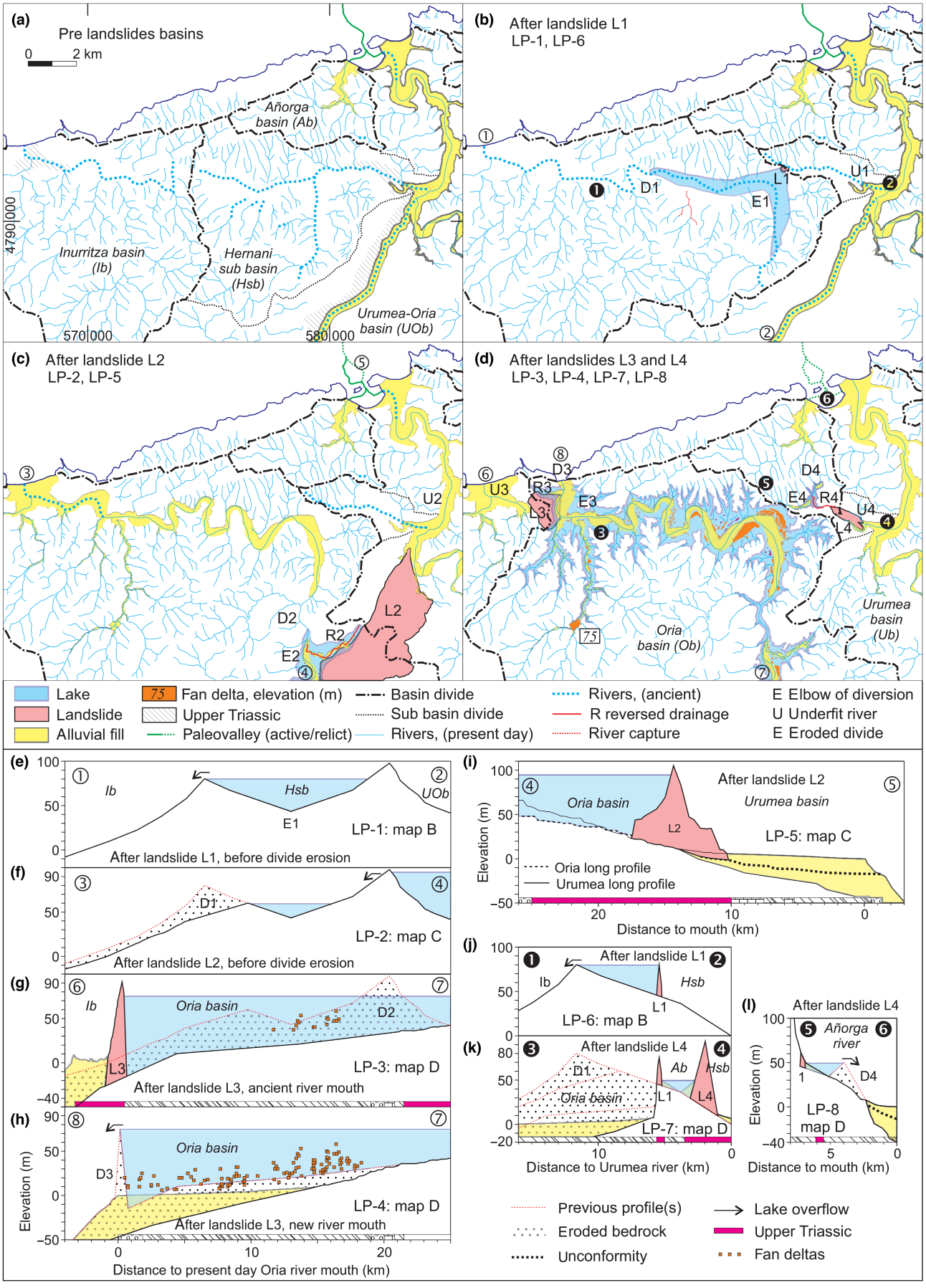

FIGURE 7 Catchment and drainage network configurations showing the evolution of the lower Oria River in four stages: (a), before landslides; (b), after landslide L1 (Irubide); (c), after landslide L2 (Atxetillun); (d), after landslides L3 (Mendibeltz) and L4 (Galarreta). Diversion-related feature labels (with numbers added) are E for elbows of diversion, D for catchment divides, R for reversed river segments and U for underfit river segments. Labels LP-1 to LP-8 correspond to longitudinal profiles drawn between the positions marked by the encircled numbers. These are shown in Figures (e–l) with the same referentials. All sections share the same horizontal scale and vertical exaggeration. See text for further details.

5.1.2 | Fluvial channel sand facies

This consists of coarse- to medium-grained sands and silt containing scarce rounded bedrock pebbles up to 4 cm in diameter and wood debris. It likely originated in relation to meandering and distributary river channels. This facies is spatially associated with the fluvial gravel facies in palaeovalley infillings, usually forming clusters of small lens-like bodies reminiscent of channel fills (e.g., Figure 4).

5.1.3 | Flood plain levee and crevasse fine-grained terrigenous facies

These consist of fine sand, silt and clay deposits with organic matter remnants (roots) and rare gravel. In the cross-sections, two sub-facies are presented: a coarser-grained (sandy) sub-facies likely related to river margin levees and crevasse splays, and a finer-grained (clayey) floodplain sub-facies. Both were deposited in floodplain sedimentary environments adjacent to river channels. This facies is volumetrically significant in the middle segment of the Oria and Urumea coastal palaeovalleys, between their infilling apex and the coastline. It is interesting to note in the Urumea palaeovalley fill that this facies is volumetrically very important (Figure 5) and contains several lenses of fluvial channel gravel and sand facies. With respect to the principal fluvial channel gravel facies bodies, the flood plain facies either overlies it or represents a frontal (lateral) transition downstream.

5.1.4 | Estuary channel gravel facies

This is made of coarse-grained sands and gravels containing clasts up to 10 cm in diameter together with shells of marine and transitional environment invertebrates, microfossils and organic matter. It is interpreted as deposited in an estuarine environment where fluvial channel material was reworked by waves. This is not a volumetrically significant facies type but is sedimentologically diagnostic of the marine fingerprint. In the Oria palaeovalley, a pair of sediment units with this facies were identified (Figure 4), reaching up to 5.9 m in thickness. They possibly represent palaeochannels currently buried either a few metres or rather deep under estuarine deposits. Other examples were identified in the Oiartzun River mouth, where a small surface channel and two buried gravel bodies can be recognized close to the coastline (Figures 4 and 5).

5.1.5 | Estuary sand, silt and mudflat facies

It consists of bioclastic and fine-grained terrigenous sediments that were subdivided into three sub-facies. The first sub-facies consists of medium- to coarse-grained bioclastic sands and organic-rich silt-enclosing siliceous pebbles (up to 2 cm in diameter). The second sub-facies type corresponds to fine sand, brown silt and clay with root and plant debris remnants. The third sub-facies type corresponds to accumulations of dark organic matter and estuarine/marine invertebrate shell fragments. This facies association is interpreted in relation to estuarine sedimentary environments, notably mudflats. The three sub-facies described are shown in separate palaeovalley transversal cross-sections (Figure 4) and grouped in the longitudinal profiles (Figure 5). Estuary mudflat deposits constitute the most important component of palaeovalley infillings of the largest catchments (Oria and Urumea) adjacent to the coastline. There they can be >40 m thick and directly overlie fluvial channel sands and gravel deposits. In the case of the smaller catchments, estuarine mudflat deposits are volumetrically small but form the greatest proportion of the facies types present (Figures 4 and 5). Sediments of this facies can attain a few tens of metres in thickness along the 2–5 km river lowermost courses, overlying either thin fluvial channel gravel deposits or the Meso-Cenozoic bedrock.

5.1.6 | Beach facies

It consists of fine- to medium-grained brown sands with shell fragments and little mud matrix. The sediments are interpreted as related to beach environments, where moderate- to high-energy waves produced biogenic fragments after shells and removed the finest terrigenous components (silt and mud). Beach facies deposits are >10-m-thick in a 1- to 2-km-wide coastal bar at the surface of the Urumea River mouth, so far mostly hidden under urbanized areas. By contrast, they are virtually

TABLE 2 Quaternary absolute age determinations compiled in the area. Coordinates referenced to ETRS98 datum.

Basin, site name, reference	Coordinates X, Y (UTM), Z (elevation, m)	Deposit facies material thickness	Number of samples, depth(s) sample facies and material(s) and method(s)	Age
Inurritza Herriko Barra Altuna et al. (1993)	566840 4792709 4.45 m	Litoral; estuarine silt clay >7.6 m	4 samples in estuarine facies: 2.15 m; 4.55 m vegetal; ^{14}C	4920–5810 years
Inurritza S-8 borehole Mendicoa (2011)	567222 4792622 4.18 m	Fluvial; litoral; estuarine Sand–silt–gravel 16 m	4 samples: ^{14}C 3.9 m, 6.2 m, vegetal, shell; estuary 13.8 m, vegetal; littoral 15.5 m, shell; fluvial/littoral	Post-1950 7340 ± 40 years Post 1950 25,260 ± 110 years
Urumea Bus station Edeso et al. (2017)	582915 4796995 5 m	Fluvial, estuarine gravel, silt, sand 17.5 m	7 samples, 6–17 m shell, wood, leaf, ^{14}C 2 samples: shell, wood, leaf, ^{14}C	2950–7565 years >43,500 years
Oiartzun P-9 borehole Irabien et al. (2020)	587732 4796492 4.1 m	Fluvial and estuarine silt, sand and mud 11.9 m	21 samples, 3.6–11.3 m shell, ^{14}C	4967–8017 years calibrated ages
Oiartzun Lezo borehole Irabien et al. (2020)	588809 4796755 3 m	Fluvial and estuarine silt, sand and mud 13.61 m	6 samples, 5.4–10.8 m shell, wood, organic matter and ^{14}C	563–7879 years calibrated ages
Oiartzun CANT15136,37,38 del Val et al. (2019)	34–41 m	Fluvial terrace (+10; +15 m)	3 samples; doubtful silty floodplain deposits, undistinguishable from soil; OSL	2.4–20.9 ky probably contaminated
Oiartzun CANT15139 del Val et al. (2019)	592506 4793846 49 m	Fluvial terrace (+ 25 m)	1 sample, 1 m depth, sand, 4 methods: ESR: Al, Ti-Li, Ti-H centre. OSL (probably contaminated)	445.3 ± 63.2 ky 403.5 ± 40.5 ky 334.3 ± 51.6 ky 26.7 ± 2.6 ky

absent in the Oria River mouth. In the case of the smallest river catchments, it is remarkable the case of the Iñurritza River, where 30-m-thick beach deposits occur in both its left and right wings, forming a 1-km-wide sand bar that extends >2 km parallel to the current coastline (the Zarautz beach). In the case of the rivers Añorga (with the 'Ondarreta' beach at its mouth, connected to the Urumea 'La Concha' and 'Gros' beaches) and Oiartzun (without beach), only minor beach facies sand deposits were drilled under anthropogenic fills in urbanized areas, or dredged at the seafloor a few metres under the current sea surface.

5.2 | Fluvial terraces/fans

Low-slope flat surfaces close to river courses that are placed distinctly above the alluvial plains were mapped as fluvial terraces. Since the sediments of stream-dominated alluvial fans and fluvial terraces may be similar (Mather & Stokes, 2016; Zhang et al., 2020), it is assumed that terraces can also represent in some cases the remains of alluvial fans. Terraces were identified in the Oria, Urumea and Oiartzun valleys (Figure 3), but not in the Iñurritza and Añorga valleys. Earthworks and urbanization transformed heavily some terraces. For this reason, mapping of their original form was achieved with available bibliographic records (Edeso, 2006; Gómez de Llarena, 1955; Santana, 1966a).

Strath terraces are the most commonly observed in current outcrops. They can exhibit a low slope towards river courses and contain a thin layer of alluvium made of gravels with large cobbles and boulders. In many cases, the latter were used as building elements in close farms and fences.

In a few outcrops and some boreholes, fill terraces were also found. The maximum fill terrace thicknesses observed are 6.6 m in the Oria basin, 8.0 m in the Urumea and 2.5 m in the Oiartzun basin. Fluvial channel gravel facies sediments were found at the base of some fill terraces, the upper part consisting of sand and silt (ascribable to levee and crevasse facies). The gravel facies can be up to 2.9 m thick in the Oria catchment. The gravel cobbles and boulders can reach 25 cm in diameter both in the Oria and Oiartzun basins (Edeso, 2006; Gómez de Llarena, 1955). del Val et al. (2019) dated Holocene and Pleistocene fluvial terraces of the Oiartzun River with various methods (Table 2).

5.3 | Marine terraces

These can be recognized as nearly flat surfaces adjacent to the coast both inland and in the currently submerged domain to depths of tens of metre. Their total area in uplifted domains is 0.36 km^2 and their elevations range between 10 and 280 m. Only soil and weathered flat rock on top were identified, but not detritic deposits. Uplifted marine terraces were recognized in the area by Edeso et al. (2014) and are well known on the Cantabrian coast to the W (Flor & Flor-Blanco, 2014). Regarding the submerged marine terraces, Santana (1966b) already identified one at −25 m, whereas Bilbao-Lasa et al. (2020) reported 12 terrace levels between −13 and −92 m. These exhibit staircase morphology with rocky floors and sea cliffs, their width usually ranges from 10 to 100 m scale.

5.4 | Other planation surfaces

Most of the flat surfaces of this type identified ('planation surfaces' in Figure 3) are located to the South of the coastal ridge and in the main valleys, occupying ca. 4 km^2. They occur at elevations between 10 and 360 m, although most of them (95%) are below 200 m (e.g., those mapped in Figure 3) and 80% between 50 and 150 m. Detritic deposits covering these surfaces were not identified and, considering their position, likely they are neither marine nor fluvial terraces; Santana (1966a) interpreted them as glacis remains. Planar surfaces developed over soft rocks are interpreted as estuarine terraces (Kennedy & Paulik, 2007), and are also are related to sea-level position (Retallack & Roering, 2012). The elevation of the aforementioned flat surfaces was inspected to track the position of ancient drainage divides and former river valleys (see Discussion).

5.5 | Submerged deltas and palaeochannels

Below the current sea level, two surface types can be distinguished: smooth surfaces in submerged areas covered by sandy sediments, and rugged surfaces where bedrock crops out at the sea floor. Morphologically, the smooth surfaces can be related to narrow palaeoriver channel infillings or broad river deltas (Figure 3, Table 1). The shape of contour lines is concave upstream in the palaeoriver channels and convex in the deltas.

In principle, the surface area of submerged deltas is expected to correlate with the area of their respective river drainage basins. In this regard, it is astounding the case of the Iñurritza drainage basin (a very small catchment with a widely distributed submarine sediment output; Figure 3). Galparsoro et al. (2010) interpreted this as an infralittoral progradating sedimentary wedge. By contrast, the large Oria River catchment presents a smaller submarine delta at its mouth, covering the part adjacent to the current coast of a palaeochannel. The latter can be still identified in the submarine bedrock further North of the most distal delta sediments. On its part, the Urumea

River presents a comparatively small delta at its current mouth, both above and below the coastline. Beyond the delta front, the rugged bedrock seafloor and finger-like sediment bodies show the scars of variably starved palaeoriver channels and by-pass conduits (Figure 3) that connect the coastal sediments with deeper (below 25–50 m depth) and wider accumulations. One of them occurs in the NW prolongation of the current Urumea River mouth. Two additional channels located further W (also identified by Edeso et al., 2017; Galparsoro et al., 2010; Santana, 1966a) exhibit a more prominent submarine topography. The current sediment distribution along them suggests they diverge from a common head area at −18 m depth. They lack so far any significant river counterpart inland. Downstream, the three channels converge into a unique, larger channel at −40 m depth that is recognizable down to −70 m. Here, it is interpreted that the centre of the three features reported and the final channel mark the position of the Urumea palaeoriver course during past periods of marine lowstand (tens of meters below current sea level). To the E of the current Urumea River mouth, a likely by-pass connects the coastal sediment area with a wide sediment-covered submarine area. The convex shape of the contour curves at its surface suggests this is a fan-like feature, but the possibility it hinders a small palaeovalley cannot be excluded.

5.6 | Underfit/overfit river reaches and elbows of diversion

As many as 15 underfit and seven overfit river reaches have been identified in the area studied, based on the geomorphic and quantitative data presented in Figures 3–5, and Table 1. Usually, the overfit reaches are identified in relation to underfit ones (i.e., the Lower Oria and Leitzaran Rivers) or are spatially related to gorges or straits. The elbows of diversion are located between underfit and overfit river reaches. The angle of river planform in the elbows of diversion is smaller than 90° in five cases and greater than 90° in two (E5 and E7 in Figure 3).

Specifically, the Urumea and Iñurritza rivers are both considered as underfit, whereas the Lower Oria River is classified as overfit. As regards the Leitzaran and Zelai Rivers, they are classified as overfit and underfit, respectively, after a comparative analysis of them (Figures 3 and 6, Table 1). The details of these comparisons are discussed further in the Discussion section. Moreover, two types of underfit river reaches have been distinguished. Reaches of the first type are located close to water divides, bear short lengths and are connected with alluvial plains in their lower section. The second type of underfit reaches are characterized by their low slope and flow over alluvial patches.

6 | DISCUSSION

In this section, it is reasoned that the present morphology of the drainage basins and the alluvial infills of the Iñurritza, Oria, Añorga, Urumea, Oiartzun, Leitzaran and Zelai Rivers can be explained by seven diversion events caused by landslides. It can be noticed that the effects of various diversion episodes overlap in the same area and are complex because, on one hand, the rivers involved are in neighbouring drainage basins and, on the other hand, three rivers were diverted twice. As a consequence, it is presented here as a discussion of the diversion events organized in three groups, in spite of the common geographical location: (1) diversions related to the lower Oria River, (2) diversions related to the Oiartzun River and (3) diversions related to the Leitzaran and Zelai tributaries of the middle Oria River (Figure 3). Geometrical details of the diversion episodes are shown in maps and reconstructed longitudinal river profiles (Figures 7–9). Regarding causative landslides and the lakes formed after river obstruction, their relevant descriptive data are presented in Table 3, whereas specific landslide cross-sections are shown in Figure 10. The landslide types involved and their possible causes are discussed in a separate sub-section. Finally, a discussion on the dating and age of the diversion events is bestowed.

6.1 | Lower Oria diversions

It can be asserted that, before diversion episodes, there existed two river drainage basins in the area occupied by the current lower Oria River (downstream of the Bazkardo gorge; Figure 3). These were the Iñurritza basin to the W (directly draining to the Cantabrian Sea) and the Hernani sub-basin to the E (a catchment of the larger Urumea River drainage; Figure 7a). Reconstruction of the ancient Iñurritza drainage basin was achieved by joining the present-day Iñurritza basin and the western drainage sub-basin of the lower Oria (Figure 3). Regarding the ancient Hernani sub-basin, reconstruction of its upper part took into account the inherited hierarchy and organization of the fluvial network recognizable so far at the headwaters of the eastern lower Oria. They support the precursory existence of an E-directed catchment drainage, although currently the drainage is to the W. Reconstruction of the lower part of the former Hernani sub-basin is constrained by the existence of a fork of the Urumea alluvial plain (with a 0.24 km^2 area) that at present is fed by a catchment of only 3 km^2 (Figure 3).

Four diversion events (here termed 1–4) transformed the organization of the ancient Iñurritza and Hernani catchments in successive steps. All those events were caused by landslides (Figure 7b–d) following this sequence:

TABLE 3 Characteristics of landslide lakes and catchment areas modified by diversion events.

Landslide number, name	L1 Irubide	L2 Atxetillun	L3 Mendibeltz	L4 Galarreta	L5 Intxaurr.	L6 Arramia	L7 Alloar
Landslide dam elevation (m)	70[a]	103	93	80	60	470	503
Fan deltas, area (km^2)	0	0.79[b]	1.20[c]	0.15	0.27	1.10	0.20
Fan deltas, elevation range (m)		45–110	6–58	35–55	7–67	400–470	450–470
Lake max. elevation (m), approx. former eroded divide elevation	80	100[d]	75	50	55	460	470
Lake area (km^2)	5	15	32	0.4	15	2.4	0.5
Lake maximum depth (m)	35	72	90	17	62	60	100
Eroded divide, present bottom elevation (m)	−15	25	−45	25	−25	375	450
Eroded divide material	Marl, limestone	Limestone	Sandstone, fault zone	Marl, limestone	Sandstone	Slate, greywacke	Dolerite, landslide
Diverted basin (km^2)	42.6	776.5	874.0	3.9	84.9	58.6	4.4
Gaining basin before diversion (km^2)	78.0	121.0	0.3	14.5	1.0	61.0	119.6
Beheaded underfit basin, after diversion (km^2)	7.4[e]	277.4	23.2	3.5[e]	2.8	38.4	34.0
Reversed underfit river catchment (km^2)	0	5.5	4.1	1.1	4.0	0	4.4

[a]Probably eroded.

[b]Upstream of Bazkardo gorge.

[c]Downstream of Bazkardo gorge.

[d]Eroded divide could at higher elevation, karstic connection.

[e]Hernani sub-basin.

TABLE 4 Characteristics of the landslides shown in Figure 11.

		Geometry				Geomorphology		Geology		
Landslide	No.	Area km^2	Thick. max. (m)	Rupture surface angle (°)	Displacement at toe (m)	Scarp, flanks and toe recognition[a]	Influence on rivers	Body material	Body contacts[a]	Upper Triassic in base
Irubide	L1	0.06	50	11.3	250	B B B	Div	C	B	Yes
Atxetillun	L2	12.3	300	4.1	750	A A A	Div, Fan	B, K, J, K	A	Yes
Mendibeltz	L3	1.4	200	7.1	450	A B B	Div, Fan	T	B	Yes
Galarreta	L4	0.50	100	12.3	200	B C A	Div, Fan	J, C	B	Yes
Intxaurrondo	L5	1.7	80	3.5	300	B A A	Div, Fan	C	C	No
Arramia-Zip.	L6	4.2	200	5.7	1000	A A B	Div, Fan	B, K	A	Yes
Alloar	L7	1.1	220	10.6	700	A B B	Div, Fan	J, C	A	Yes
Otaburu	L8	0.43	100	26.6	400	A B C	Dam, Fan	B	B	Yes
Banderagaña	L9	0.52	200	6.8	150	A B B	Def	K, C	C	Yes
Olaskogaña	L10	1.8	100	2.9	100	B B C	Nar, Def	C, T	C	No
Aingeru G.	L11	10	70	4.2	100	C B B	Nar, Def, Fan	C	C	No
Basozabal	L12	0.90	100	4.4	100	B A A	Nar, Def	C	C	Yes
Antondegi	L13	1.1	80	3.7	300	B A A	Nar, Def	K, J, C	A	Yes
Urkabe	L14	2.2	150	3.8	150	B A A	Nar, Def	K, J, C	B	Yes
Larrainburu	L15	2.3	80	5.2	300	A A A	Nar, Def	K, J, C	A	Yes
Izaskun	L16	1.8	70	9.3	200	B A A	Nar, Def	K, J	B	Yes
Aiete	L17	10.1	100	1.9	300	B B B	Nar, Def	C	C	No
Ipuliño	L18	1.5	70	20.6	0	A A C		P, B, K	B	No
Iskibi	L19	0.48	100	14.9	100	A A B	Dam, Fan	P	B	No
Arraia	L20	0.10	30	18.4	50	A B C	Dam, Fan	K, J	A	Yes
Alkiza	L21	0.15	30	23.8	100	A B C	Dam, Fan	B, K	B	Yes

Abbreviations: Dam, damming; Def, deflection; Div, diversion; Fan, fan deltas; Nar, valley narrowing.

[a]A: clear, B: plausible and C: uncertain.

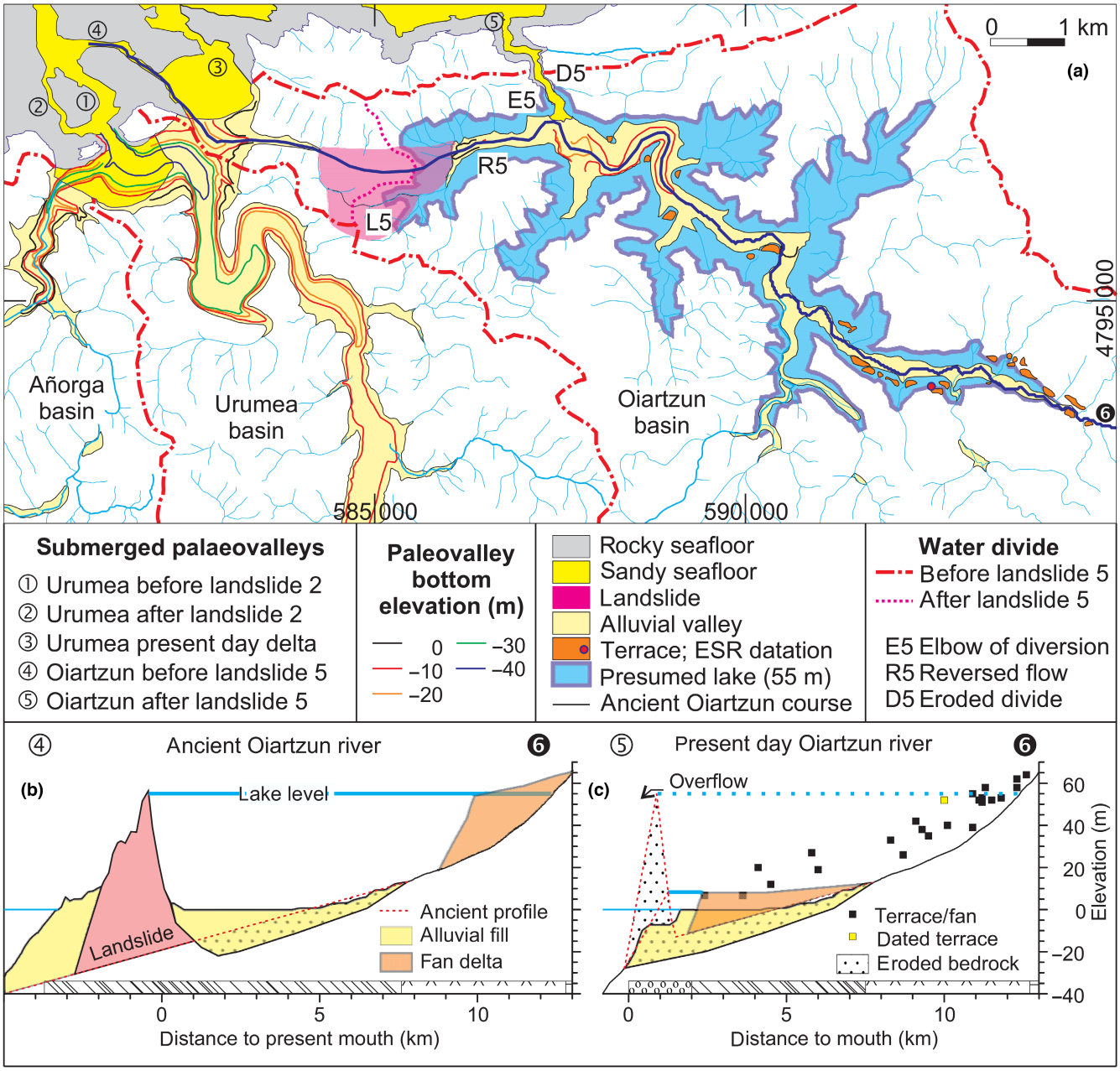

FIGURE 8 Catchment and drainage network configurations of the Oiartzun basin (a) and reconstructed longitudinal river profiles (b and c) between the reference points denoted with encircled numbers. The profiles share horizontal scales and vertical exaggerations. See text for further details.

the Irubide landslide (L1 in Figure 7b), the Atxetillun landslide (L2 in Figure 7c), the Mendibeltz landslide (L3 in Figure 7d) and the Galarreta landslide (L4 in Figure 7d).

6.1.1 | Diversion 1 (Irubide landslide)

This event was inferred to have occurred in the central part of the Hernani sub-basin of the antecedent Urumea–Oria drainage basin (Figure 7a), caused by a landslide at Irubide (Figure 7b). The area occupied so far by L1 is 0.06 km^2 (Figures 7b and 10, Table 4). It affected Albian siltstones (Figure 2) that partly glided over Triassic evaporites currently cropping out in the valley thalweg. In detailed geological maps of the area (Campos & García-Dueñas, 1974), the landslide boundaries are not traced, but an already mapped mechanical contact coincides with its toe. In spite of this, morphologically the landslide body can be identified as a hill that a century ago was bounded by small roads at the headscarp and the toe. Currently, the hill appears disfigured and occupied by a road junction complex. The headscarp's slope is 22%. It can be estimated that the vertical displacement component of the landslide was

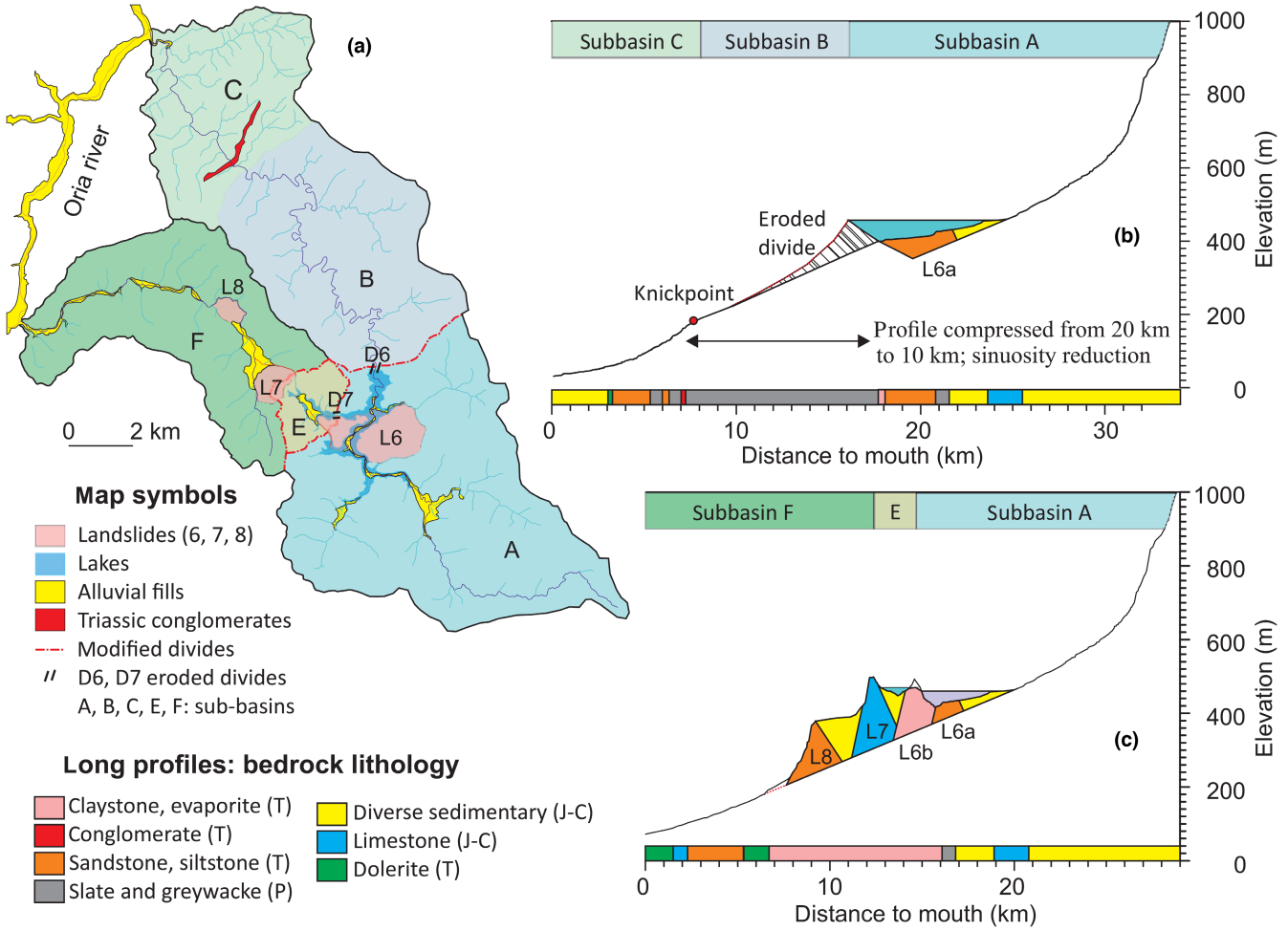

FIGURE 9 Catchment and drainage network configuration reconstruction (a) and longitudinal profiles for the Leitzaran (b) and Zelai (c) Rivers. The profiles share horizontal scales and vertical exaggerations. See text for further details.

of the order of 40 m, whereas the horizontal displacement at the toe reached 250 m.

The geomorphic supporting evidence of diversion consists firstly in the presence of an elbow of diversion (E1 in Figure 7b) and secondly in the identification of an eroded divide (D1). The diversion elbow is located at the former confluence of two forks of the precursory Hernani River (Figure 7a). So far, the Oria River valley and its alluvial plain are wider at the elbow, compared with counterparts at the upstream and downstream reaches (Figure 3). At the eroded divide, the current Oria River course is incised and the alluvial plain is very narrow. Additionally, the planation surface relics in the surroundings suggest that a former divide with an elevation of ca. 80 m existed in this area.

The Irubide landslide caused a river obstruction and formation of a lake with an estimated elevation of 80 m (see Table 3 for further details and longitudinal profile LP1 in Figure 7e). The lake elevation estimation is constrained by those of the former divide D1, on one hand, and of the landslide dam crest (currently 70 m, possibly due to its partial erosion). Identification of fan delta deposits at elevations around 80 m inside the catchment was not achieved. This absence might be either a consequence of the small catchment areas of the tributary rivers that reached the lake or due to a low preservation potential (erosion after their formation).

The diversion originated in the Hernani River reduced its drainage basin surface from 50.0 to 7.4 km^2. Downstream the obstruction, its original course turned into an underfit river (U1 in Figure 7b) that was subsequently modified by another landslide. At the same time, the Iñurritza River catchment increased its surface area from 78 to 121 km^2, the likely increased stream power eroding further the head of the ancient Hernani River. This would have caused capture and flow reversal of one river branch (Figure 7b).

6.1.2 | Diversion 2 (Atxetillun landslide)

The Atxetillun landslide (L2 in Figure 7c) is a large feature, with an area of 12.3 km^2, a slab configuration and a

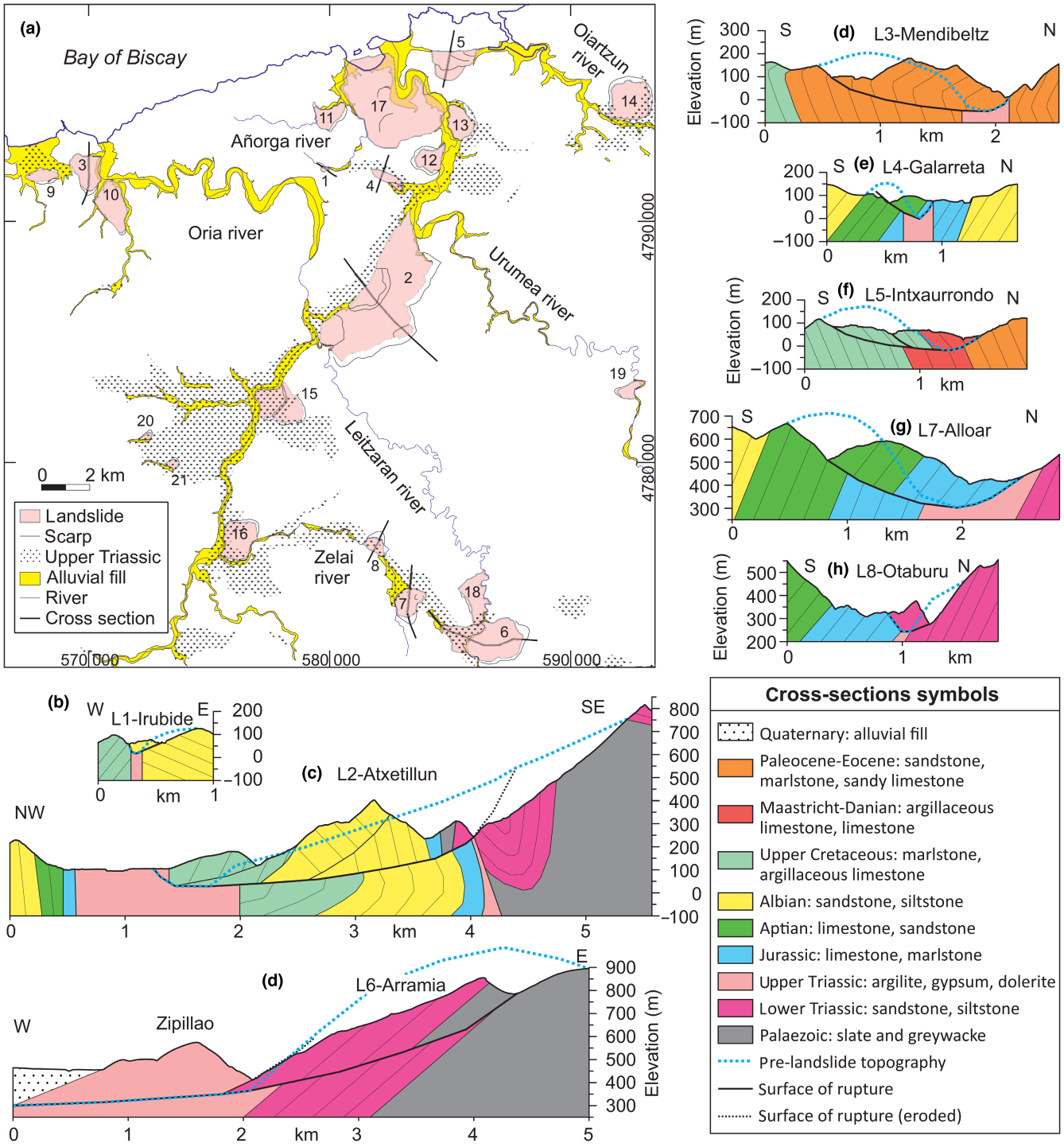

FIGURE 10 (a) Sketch map showing the distribution, shape and size of significant landslides (labelled L1–L21) disclosed in the area studied. Straight segments labelled 1–7 correspond to the geological cross-sections of the river-blocking landslides discussed in the main text with further detail, shown in Figures (b) (landslide L2, Atxetillun), (c) (L6, Arramia–Zipillao), (d) (L3, Mendibeltz), (e) (L4, Galarreta), (f) (L5, Intxaurrondo), (g) (L7, Alloar) and (h) (L8, Otaburu). The cross-sections share identical horizontal scales and vertical exaggeration x2. Landslides L9–L21 are non-blocking landslides and deep-seated gravitational slope deformations (DSGSD). See text for further details.

maximum thickness of ca. 300 m. It embraces two smaller landslides nested in the main body (Figures 3 and 10, Table 3). It is formed mainly by Mesozoic sedimentary rocks, with Triassic evaporites at the toe. The slide surface cuts lithological contacts and bedding at a high angle. Mapped boundaries are marked by faults and mechanical contacts (Campos & García-Dueñas, 1974). Current streams follow these headscarp, flank and toe contacts. This landslide is here interpreted as being younger than L1 because, otherwise, the diverted ancient Oria–Urumea

River would have flowed back into the Urumea River through the Hernani River.

The L2 landslide caused diversion of the ancient Oria–Urumea River. A stream obstruction formed a lake with a surface elevation of ca. 100 m. This is supported by the preserved elevation of the landslide dam crest and by the common elevation of several fan delta top set deposits (Table 3). In this regard, wide areas of the middle Oria basin alluvial plain can be considered as the remnants of previously confined (Nemec & Steel, 1988) fan deltas (Figure 3), the dissection of which gave rise to deposits that might be interpreted as fluvial terraces on geomorphic grounds (Zhang et al., 2016) but that genetically are not. The original minimum elevation of the divide between the Urumea–Oria and Iñuritza Rivers might have been higher than the lake level. However, there may have been a karstic underground connection between the lake and the transient Iñurritza basin that likely facilitated the divide reconfiguration. Erosion of the divide at site D2 from Figure 7c gave rise to formation of the Bazkardo gorge (Figure 3). The Oria River, which previously flowed from SW to the NE over Triassic evaporite bedrock, twisted its course northwards forming an elbow of diversion (E2; Figure 7c) and crossed the Bazkardo limestone gorge. The short river segment between the landslide dam and the diversion elbow E2 (segment R2 in Figure 7c) associates a valley bottom 250 m wide and a gradient of 0.9% in its middle part (too low to be located at a catchment head). It is interpreted here that it constitutes an underfit reversed river that occupies the ancient Urumea–Oria valley. Its current lower segment was also blocked in part by the Atxetillun landslide, causing a change in its valley direction from NE–SW at the head to SE–NW downstream.

Due to erosion of the divide at D2, the former Iñurritza basin experienced a renewed catchment area increase from 121 to 897 km^2. After the diversion, the new Oria River might have initially fed the lake dammed by the partially eroded divide D1 (Figure 7a), forming fan deltas the relics of which are currently found at elevations between 40 and 58 m (longitudinal profile LP-2; Figures 3 and 7f). Towards the coast, the new Oria River promoted increased incision, first in the Iñurritza palaeovalley and then in its palaeovalley upstream.

Downstream of the L2 landslide (Figure 7c), it is interpreted that the lower reach of the former Oria–Urumea River became underfit (U2 in Figure 7c). The facts that the Oria and Urumea palaeovalleys are similar in size and slope, and associate basal gravel beds of comparable thickness (Figure 5a,b, Table 1), suggest that both palaeovalleys were generated by fluvial systems of similar size (Blum et al., 2013; Gibling, 2006; Wang et al., 2019). The Urumea River underfit condition is also noticed because in the alluvial plain, the river is laterally unconfined (with complete alluvial channel boundaries), in contrast to the Oria River alluvial plain, which flows over a valley partly confined by rocky boundaries (Fryirs & Brierley, 2013).

The ^{14}C datings of the Urumea palaeovalley (see Table 2 and references therein) suggest that there exists a hiatus in the Quaternary sedimentary record at elevation of −9 m (2.95–7.65 ky above and >43.50 ky below).

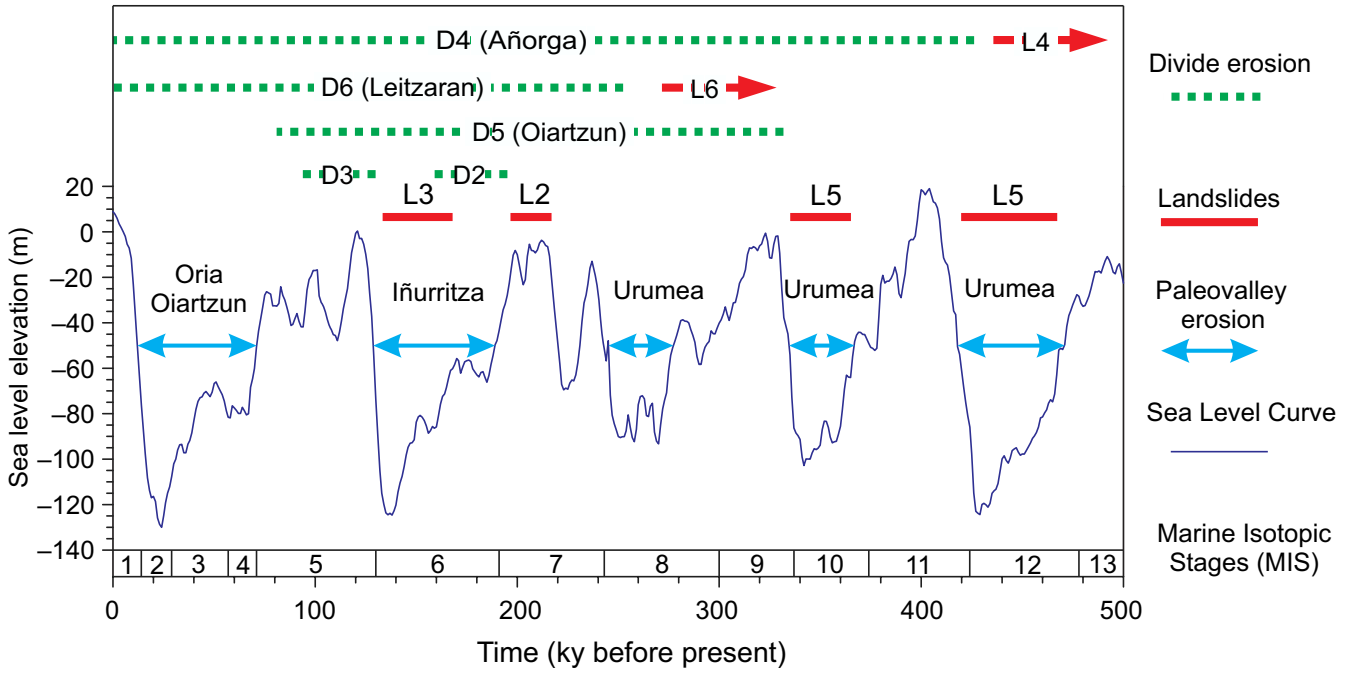

FIGURE 11 Dating of landslide events, periods of palaeovalley incision and divide erosion stages in the chronological reference framework provided by the sea level elevation curve from Spratt and Lisiecki (2016). See text for further details.

The gap can also be inferred in other parts of the palaeovalley infill, as there are two gravel beds at different elevations (Figure 5b). It is interpreted here that the hiatus could have been caused as follows. First, the stream flow of the Urumea River was reduced by diversion (coinciding with a sea-level highstand stage). Then, during a subsequent sea-level drop, the Urumea River eroded partly its former (late Pleistocene) palaeovalley fill. Finally, during Holocene sea-level rise, the partially eroded palaeovalley was infilled again, forming the stratigraphic gap.

The footprint of diversion can be tracked in the present submerged domain of the Urumea River mouth, too. There exist three submerged palaeoriver channels there (Table 1; Figures 3 and 8a). Likely, the central one (the widest) pre-dated river diversion. The western palaeochannel would post-date diversion. Avulsion of the original river channel likely led to decreased flow of the Urumea River, also allowing coastal dynamics to build a barrier. The western and central palaeoriver channels diverge at a depth of −18 m. It is envisaged that this zone might be genetically related to the stratigraphic hiatus discussed above (although other relationships might also exist). The eastern palaeoriver channel origin is discussed further in Section 6.2, related to diversion events in the Oiartzun River.

6.1.3 | Diversion 3 (Mendibeltz landslide)

The Mendibeltz landslide (L3; Figure 7d) displaced the mouth of the Oria River from the Iñurritza Valley to its present position. The landslide has a surface of 1.4 km^2 and a maximum thickness of 200 m. The vertical displacement is ca. 70 m and the horizontal displacement at the toe is ca. 450 m (Table 3). The landslide headscarp and body are formed by late Cretaceous and Cenozoic sandstones and marlstones, while at the toe Triassic evaporites crop out. In detailed geological maps of the area, the western landslide flank and a secondary scarp are tracked by faults with slip components coincident with those expected for a gravitational landslide (Campos & García-Dueñas, 1974; Garrote et al., 1988; Hanisch, 1974a). The headscarp is still partially recognizable, the western flank and the toe being followed by small creeks. This landslide should be younger than L2 because no other river than the Oria could have eroded the Iñurritza palaeovalley at the slide site.

The Mendibeltz landslide formed a lake (32 km^2 in area; Table 3) with an elevation of ca. 75 m, constrained by the elevation of the dam crest (93 m) and by that of fan delta remnants preserved in a branch of the current lower Oria (Figure 7d). This is also the elevation of wide areas of the alluvial plain of the middle Oria upstream of the Bazkardo gorge, which would have been transiently submerged enabling extension of the lake to the S (Figures 3 and 7d). The lake overflow would have eroded the divide close to the coast at site D3, facilitated by a fracture zone (Hanisch, 1974b). Progressive divide erosion permitted river incision and the punctuated formation of additional fan deltas at elevations below 75 m both in the middle and the lower Oria sub-basins (Figure 3, Table 3). In the case of the middle Oria (upstream of the Bazkardo gorge), the fan deltas at elevations below 75 m (e.g., those between 40 and 58 m) were also formed during drainage of the lake created by L2 (with an initial 100 m elevation). These were later reworked in the lake created by the L3 landslide. In the case of the lower Oria, fan deltas located at elevations between 6 and 58 m (Figure 3, Table 3) formed while the divide was eroded.

The course of the ancient river can be traced to the E and W of the L3 landslide. To the W, it forms a wide and deeply incised fork of the beheaded Iñurritza alluvial valley (U3 in Figure 7d), which could not have been eroded by its current small river (Figure 3). To the E, the river traverses a broad valley with a negligible creek that corresponds to a reversed underfit river segment (R3 in Figure 7d). The elbow of diversion E3 is located 1.5 km upstream of the current Oria River mouth. The ancient river was 3.5 km longer than the present day.

The Iñurritza palaeovalley infill lacks the basal gravel bed present in the palaeovalleys previously discussed (Urumea, Oria and Oiartzun). It is interpreted here that the L3 landslide (with its base 20–30 m below the current sea level; Figure 7g) occurred during a lowstand sea-level period, while the palaeovalley was being eroded and carried, at most, a thin gravel bed in the channel (Sklar & Dietrich, 2006). During the sea-level rise, the wide underfit river (U3 in Figure 7d, now a littoral palaeovalley) did not associate fan deltas with gravel deposits and was replenished with estuarine and beach sediments.

6.1.4 | Diversion 4 (Galarreta landslide)

The Galarreta landslide (L4 in Figure 7d) occurred in the remainder of the Hernani River after being beheaded by the diversion caused by the L1 landslide. The L4 is slab shaped, with 0.5 km^2 of surface area. It is made mostly of Aptian limestones (Table 4). The headscarp and the toe are tracked by two streams draining to the Urumea basin, and are identified as mechanical contacts in detailed geological maps of the area (Campos & García-Dueñas, 1974). This slide is interpreted as younger than L1 because the fan deltas it formed overlap the fan deltas and the beheaded palaeovalley associated with the L1 landslide (Figure 7d,j).

The inferred river diversion (E4; Figure 7d) can be recognized by the anomalous channel network pattern of the Añorga River (Figure 3). A short river segment flows from W to E over soft Triassic evaporites very close and parallel to the water divide between the Añorga and Urumea basins, but at the elbow of diversion (E4 in Figure 7d) the course abruptly changes to the N direction. Then the river traverses a strait composed of upper Cretaceous soft marls and hard limestones (D4 in Figure 7d). The Añorga River longitudinal profile (Figure 5c) shows a significant contrast between its right (southern) and left (northern) branches. The right branch presents a reduced gradient between 30 and 50 m elevation in the upper part of the basin that the left branch lacks. Additionally, the low-gradient area contains two patches of alluvial deposits that are interpreted as confined fan deltas (Nemec & Steel, 1988; Figure 3, Table 3), based on the small area of Añorga River (about 4 km^2) at site of the alluvial deposits.

The L4 landslide blocked the valley of the tributary river and formed a small lake (0.44 km^2; Table 3) with an elevation of about 50 m. This is also the elevation of the highest fan deltas preserved (Figures 3 and 7d,j,k). When the D4 divide was eroded, a Hernani River segment (R4) reversed between the landslide and the diversion elbow. As a result, the former course of the river was modified by avulsion due to the presence of fan deltas. Upstream L4, the former Hernani River segment R4 is as well an underfit river with low slope (1.14%) and a small watershed (1.13 km^2). Downstream L4 in the Urumea catchment, the diversion event can be detected by the presence of a broad valley and alluvial plain associated with a short tributary (an underfit rivulet, U4 in Figure 7d).

6.2 | Oiartzun River diversion (Intxaurrondo landslide)

The former Oiartzun River flowed over Eocene marls in an E–W direction, its ancient mouth coincided with the easternmost submerged palaeovalley in the Urumea River mouth area (Figures 3 and 8, Table 1). At the coast, the palaeoriver channel is buried beneath the Urumea River delta. Further E, the ancient Oiartzun palaeovalley is now a 100-m-wide arm of the Urumea alluvial plain with a small culverted stream. The culverted stream is the underfit river (U5 in Figure 8a) downstream of the Intxaurrondo landslide (L5).

The L5 landslide body has an area of 1.7 km^2 and a maximum thickness of 80 m. It is formed by late Cretaceous and Palaeogene marl and limestone alternations (Table 3). Although it has not been identified so far in geological maps by means of mechanical contacts at their boundaries, it can be recognized through a geomorphic criterion: the landslide is bounded by a partly eroded main headscarp. In detail, the headscarp was occupied by two diverging ravines, and a secondary scarp parallel to it can be also defined by two other gullies.

East of L5, the precursory Oiartzun River associates a palaeovalley fill that reaches the elbow of diversion (E5 in Figure 8a). This alluvial infilling (1 km long and 200 m wide, but with only 4 km^2 of catchment area) traces the underfit valley segment (R5; Figure 8a) formed by flow reversal of the ancient Oiartzun River. East of the elbow of diversion, the current Oiartzun River valley is 250 m wider than the palaeovalley of the reversed river.

Likely, L5 formed a lake based on the presence of gravel deposits in the Oiartzun valley. The deposits were previously interpreted as terraces deposited in a high-energy stream (Edeso, 2006). However, because they occur in a relatively small basin area (12 km^2) where the channel slope is 1.7%, we interpret them as fan deltas eventually deposited in the lake margins. The lake elevation (60 m) is constrained by elevations of the current landslide crest dam and the highest terraces (Figure 3, Table 3). The lake overflowed into a coastal creek at position D5 in Figure 8a. There, it incised a pre-existing divide composed of hard siliceous sandstone until a gorge was formed.

The reconstructed profile of the ancient Oiartzun River (Figure 8b) can explain the reason why the depth of its palaeovalley (−25 m) is shallower than the depth of the Oria and Urumea palaeovalleys (−45 to −50 m). It can also explain the similar slope of those three rivers in their lowest reaches. The reconstructed profile, when compared to the current (Figure 5e), permits us to explain the occurrence of a knickpoint ca. 3 km from the coastline. It is envisaged here that, before diversion, the former river mouth likely formed an equilibrium profile in connection with the upper part of the present Oiartzun River (Figure 8b). After diversion (Figure 8c), erosion of the hard rock divide (D5) would have needed a long time, with faster incision rates occurring only during sea-level lowstand stages. Likely, divide erosion completion would have been achieved when sea level was below modern. Since the river cannot erode its bed at the bottom of the lake, during divide erosion, the ground elevation increased by uplift. After complete incision of the water divide, a knickpoint started to develop and move upstream, removing first the soft materials of the lake-infilling alluvium. As a consequence of diversion, the river length was shortened by 3.7 km, and the resultant longitudinal profile slope increase also contributed to development of the knickpoint.

6.3 | Leitzaran and Zelai River diversions (Arramia–Zipillao, Alloar and Otaburu landslides)

The Zelai and Leitzaran tributaries of the Oria River (Figure 3) exhibit anomalous drainage network characteristics. These include the following: (1) Based on the relationship between the floodplain and the basin area in its lower reaches (Table 1), the Zelai River is underfit while the Leitzaran River is overfit. (2) The longitudinal profiles of the Zelai and Leitzaran rivers (Figure 6) indicate low gradient segments in their upper reaches compared to their mouths, along with wide alluvial plains in their headwaters. A geophysical survey of one of the alluvial deposits in the upper reach of the Zelai River revealed a thickness of almost 100 m (EVE, 1996). (3) In the middle reaches of the Leitzaran River, there is a 20-km-long section with high sinuosity upstream of a knickpoint (Figures 3 and 6). (4) A significant segment of the drainage divide between the Leitzaran and Zelai basins coincides with continuous outcrops of soft evaporitic rocks.

The anomalous drainage network attributes can be explained by involvement of three landslides. Two landslides (L6 and L7) caused river diversion, and the third landslide (L8) caused river damming without diversion. The Arramia–Zipillao landslide (L6 in Figure 9) occurred in the upper part of the former Leitzaran–Zelai River, at the junction of its main branches. The landslide (4.2 km^2 in area; Table 4) involved mass transport (with a maximum thickness of 200 m) towards the main river channel downstream of the fork confluence and blocked the valley. The landslide has two parts (Figure 10c): the Arramia block in the upper part (formed by Triassic red sandstones), and the Zipillao block in the lower part (formed by dolerites). In detailed geological maps of the area, the landslide boundaries coincide with mapped minor faults and mechanical contacts. The position of the main headscarp is recognizable in the current terrain by a geomorphic saddle. The flanks are followed by small rivers. So far, the Leitzaran River flows through the secondary scarp of the landslide, which separates the Arramia and Zipillao blocks. Vertical displacement is ca. 100 m at the principal headscarp and the horizontal displacement is ca. 1 km at the toe (Figure 10c). The landslide raised the thalweg of the precursory Leitzaran River as it flowed over, creating the recent low slope reaches at 420–450 m elevations (Figure 6a).

The elevation of the lake formed by landslide L6 was ca. 470 m, constrained by elevations of the landslide dam crest and of the highest fan deltas (Figure 3, Table 3). The lake spilled over the ancient divide between sub-basins A and B from Figure 9 at a location dominated by slates and greywackes, forming there an incised narrow part of the current Leitzaran valley. Downstream of this eroded divide, the precursory Leitzaran River catchment had two parts separated by a knickpoint (at a distance of 7 km of the mouth) in an area dominated by hard Triassic conglomerates (Figures 6a and 9b). The headwater part flows over soft Palaeozoic low-grade metamorphic rocks, whereas the lower part flows mainly over Mesozoic sedimentary rocks lithologically diverse. After diversion, the ancient Leitzaran almost doubled its area (Table 3) and the resultant Leitzaran River experienced a reduction in its average slope. This might have induced the development of sinuous meanders (e.g., Johnson & Finnegan, 2015) as the river coursed over soft Palaeozoic bedrock (Figure 6c). In the reconstructed longitudinal profile of the ancient Leitzaran River (Figure 9b), sinuosity was removed, thus reducing its length from 20 to 10 km in the sub-basin B. This way the thalweg slope connects smoothly with the headwater river profile.

As a consequence of diversion caused by the L6 landslide, the precursory Zelai River basin lost 45% of its area in the upper catchment and became an underfit river. The resultant Zelai River catchment incorporates two additional landslides: the Alloar and the Otaburru landslides (L7 and L8, respectively, in Figure 9a).

The L7 landslide (located at the catchment head) dammed the river and created a lake with an elevation of ca. 462 m. The landslide body has a surface of 1.1 km^2 and a maximum thickness of 220 m (Table 4). It is formed mostly by Mesozoic limestones, but Triassic evaporites crop out on the valley floor (Figure 10g). The landslide headscarp is well preserved, marked by two gullies. A secondary landslide can be identified at the toe. The estimated landslide vertical and horizontal displacements are ca. 120 and 700 m respectively. The lake that resulted after river damming was subsequently filled with fan delta sediments. A low slope, underfit and reversed rivulet eventually flowed over it. Diversion was achieved through erosion across the older L6 landslide at an incised geomorphic feature connecting the sub-basins E and A in Figure 9a. This led to incorporation of ca. 4 km^2 of the ancient Zelai headwaters (Table 3) into the Leitzaran River drainage basin.

The L8 landslide (located at the central area of the catchment; Figure 9a) blocked the Zelai valley and formed a lake that was filled by fan delta sediments preserved to date. The lake had a surface of 11.4 km^2 and the thickness of the sediment fill attains ca. 100 m (EVE, 1996). The landslide body is formed by Triassic red sandstones, has a surface area of 0.43 km^2 and a maximum thickness of 160 m (Table 4). Vertical and horizontal displacements of 200 m at the scarp and 400 m at the toe, respectively, can be determined (Figure 10h). It does not exhibit explicit tectonic boundaries in geological maps. However, up- and downstream of L8 soft rocks of distinct nature (Triassic evaporites) crop out in the valley bottom. Therefore, the corresponding lithological contacts can be correlated with

the landslide lateral limits. So far, the most evident geomorphic feature of the landslide is its headscarp, the Zelai River flowing between the landslide body and the bedrock scarp.

Relative dating of L6, L7 and L8 landslides can be established through overprinting relationships with respect to their associated fan deltas (Figure 9c). L6 is overlain by fan delta deposits formed upstream of L7. The latter, in turn, is overlain by fan delta deposits formed upstream of L8. It is also remarkable to note that valley blocking and the upstream infilling caused a reduction in landslide likelihood in this area.

6.4 | Landslides as a cause of river diversion and landslide triggers

So far, attribution of the cause of river diversion to landslides has not been straightforward. As a matter of fact, in this study, given the close association of Triassic evaporites with river diversion segments, the option first explored was diapiric remobilization. This appeared reasonable as well in view of previous studies on similar geological situations (Colman, 1983; Gutiérrez et al., 2019). A major drawback of the hypothesis, however, is that in order for diapiric remobilization to be capable of diverting rivers, the induced local uplift should exceed the erosion rate. No such evidence was found in large rivers such as the Oria and, thus, the hypothesis was discarded.

The correlation among evidence of diversion in the drainage network, geomorphic specific features, Quaternary sediment organizations and geological contacts in the water divide areas was the actual clue that led to terrain re-inspection and then to detection of a number of landslides that blocked river valleys. Seven of the eight valley-blocking landslides discussed to this point were found to have caused river diversion. Notwithstanding, another 13 landslides identified had variable impacts on fluvial drainage network dynamics (L9–21 in Figure 10a). Some of them bear dimensions (Table 4) comparable to those of giant landslides described elsewhere (e.g., Delchiaro et al., 2019; Hancock & Perrin, 2009). Taking into account the power-law magnitude/frequency distribution unravelled by Hovius et al. (1997), lots of smaller landslides may exist in the studied area, several of which were discerned during terrain geomorphic inspection.

The principal landslides studied in detail herein share a number of geological and geomorphic characteristics. First, the slid masses (affecting large parts of hillslopes) mostly maintained an internal cohesion (evidence of transformation of landslides into debris avalanches was not recognized, maybe biased by the poor outcrop quality). This might support considering them as slow-moving landsides that under the influence of external triggers turned into fast-moving landslides (Lacroix et al., 2020). The landslides are mainly translational, with minor rotational components. Their headscarps (usually simple) are disfigured by subsequent erosion in a rugged mountain region affected by a rainy temperate climate. Landslide flanks or lateral scarps usually form creeks followed by minor streams. The toes of the non-diverting landslides deflected the thalwegs and the alluvial valley plains (narrowing palaeovalley widths), whereas toes of diverting landslides (blocking palaeovalleys and damming rivers) are tracked by manifest abnormal mechanical contacts.

Most of the landslides have boundaries that coincide with minor faults or mechanical contacts represented in geological maps, as already observed by Hart et al. (2012). The lithologies of landslide main bodies are composed of various bedrock geology units, but it is common the occurrence of evaporitic Triassic rocks at their base (71% of the landslides). Delineation of the landslide rupture/slip surfaces after topographic cross-sections (joining scarps and toes) results in inclination angles ranging between 2° and 35°, with a 5° average (Figure 10b–h). The thickness of landslides ranges from 50 to 300 m (averaging 200 m), and is correlated with their surface area (Jaboyedoffa et al., 2020; Table 4).

The landslides studied herein exhibit scarp and flank morphologies compatible with deep seated gravitational slope deformations (DSGSD; Agliardi et al., 2012). Notwithstanding, at variance with DSGSD, they record displacement evidence at the toe and bear identifiable mechanical contacts in their boundaries. The existence of low-gradient landslides is similar to the observed in spreading DSGSD (Discenza & Esposito, 2021) and in large landslides from areas of relatively moderate relief (Pánek, 2022). It is possible that the landslides were originally slow-moving DSGSD actually accelerated along discrete slip surfaces or deformation localization shear zones (Lacroix et al., 2020; Pánek & Klimeš, 2016).

The causes of landslides can be diverse. Apart from suitable slopes and critical shear stress at landslide bases, the principal triggers are storms and earthquakes (Densmore & Hovius, 2000; Meunier et al., 2008). Valley incision is a common slope-increasing factor. Incision may be magnified by increasing flow through fluvial capture in drainage basin headwaters, or by lowering sea level in coastal areas. Lithological and structural factors can also contribute. Several of the favourable situations described by Stead and Wolter (2015) are met in the area studied, such as appropriate angle between potential rupture surfaces and lithological contacts and rock internal anisotropies (bedding/foliation), or existence of potential detachment surfaces at key places (Triassic evaporites). These are present in

the geological structure of many landslides (Figure 10). Storms and/or heavy rainfall are potential landslide triggers since they are frequent in the area to date. However, their role in accelerating slip in sliding masses tens to a few hundreds of metres thick (as several of the landslides studied) might be limited. Regarding earthquakes as landslide triggers, they are envisaged as a viable cause as long as they are relatively common in the area (see Section 2), even in recent times (the latest decades with instrumental monitoring records). Earthquakes are both mid-crustal and (usually) shallow, and even in the latter case, their magnitude distribution (M1 to M4) extends throughout the whole range monitored. Finally, the epicentres of some recorded seismic events coincide with or are close to landslide sites and current river valleys (Figure 2), possibly denoting ongoing slow slip at places.

6.5 | Dating of diversion events

A chronology of landslide events is tentatively put forward using a combination of relative and absolute dating methods (Table 2). Using geometric relationships between geomorphic features, three landslide sequences can be inferred. In the lower Oria River basin, from older to younger, there are two concatenations: landslides L1 (Irubide) – L2 (Atxetillun) – L3 (Mendibeltz) and L1 (Irubide) – L4 (Galarreta). In the middle Oria catchment, the progression was: landslide L6 (Arramia-Zipillao), L7 (Alloar) and L8 (Otaburu). The geometric relationships cannot be used to establish connections among the three landslide sequences and with the landslide L5 (Intxaurrondo) of the Oiartzun catchment. In spite of the above, absolute age dates available and additional relative dating criteria can shed more light, as explained below (Figure 11).

It is envisaged that the oldest Urumea palaeovalley fill should have formed during Marine Isotope Stages MIS-8/7 (337–243 ky). Since the river diversion caused by the landslide L2 likely occurred during a sea-level highstand, and the Oria River eroded two palaeovalleys after its diversion, L2 likely occurred during the MIS-7 (243–191 ky interglacial). The Iñurritza palaeovalley erosion period during the MIS-6 (191–130 ky glacial stage) would have included the L3 landslide event. The current Oria palaeovalley would have been eroded during the MIS-2 stage (29–14 ky). This is supported by the unconformity disclosed in the Urumea palaeovalley fill, separating Pleistocene sediments >45 ky underneath from Holocene ones (7.6–2.9 ky) above −9 m.

The fan delta formed by landslide L5 at 50 m elevation was dated between 508 and 284 ky (del Val et al., 2019). Since L5 is located on a submerged palaeovalley, it appears reasonable to consider that the landslide might have occurred during a low sea-level stage. Therefore, it might be ascribed to MIS 10 (374–337 ky) or MIS 12 (478–424 ky; Figure 11). After the ancient Oiartzun River was diverted, the divide and the palaeovalley were eroded one after another (Figure 9). The divide incision above sea level was 55 m, whereas palaeovalley incision below sea level was 25 m. The former should have been eroded at a lower rate than the latter since streams in the divide have no gravel to erode (Garcia-Castellanos & O'Connor, 2018). Thus, it is envisaged that the divide incision lasted until MIS 6 (191–130 ky) or MIS 4 (71–57 ky) and the palaeovalley incision extended till MIS 2–3 (57–14 ky). The shallow depth of the Oiartzun palaeovalley (−25 m) possibly was due to combination of hard siliceous conglomerate bedrock and a relatively short incision interval. The fact that the Urumea and Iñurritza palaeovalleys do not show evidence of uplift, in contrast with the Oiartzun palaeovalley, points to L5 being older than L2. The possible Cantabrian Mountains uplift rate decrease during the Pleistocene (Benito-Calvo et al., 2021) might also explain the point of the aforementioned palaeovalleys.

In order to approximate the minimum age of the L1, L4, L6 and L7 landslides, it is accepted that lake overflow caused divide incision at the top and front, similar to landslide dam erosion (Zhonga et al., 2020) and to knickpoint recession. Loget and Van Den Driessche (2009) estimated that knickpoint recession rate is proportional to the square root of basin area. Following this approach, the divides D6 and D5 should have retreated at similar rates, about five times faster than divide D4. This simplistic approach does not consider the thickness, length and hardness of the eroded divide bedrock. However, it highlights that the L4 and L6 landslides pre-dated L2 in the Oria catchment. Regarding the eroded divides D2 and D3, they should have retreated nine times faster than D5. Thus, L2 and L3 should be younger than L5, as inferred above. This reasoning cannot be applied to relate divides D1 and D7 because the first was eroded by overflow of the lakes formed by landslides L1 and L2, whereas D7 was incompletely eroded.

7 | CONCLUSIONS

A geological and geomorphic framework of diagnostic criteria was used to detect river diversion by landslides in the western Pyrenees, including identification of elbows of diversion, eroded divides, beheaded underfit rivers, diverted overfit rivers, reversed river segments and large landslides. River blocking landslides modified original and transferred (diverted) drainage networks both up- and downstream. The Oria drainage river basin's case suggests that river diversions due to landslides

were likely more frequent than previously presumed, and might be significant in mountainous areas of moderate relief elsewhere.

In the study area, some landslides caused the formation of lakes that overflowed upstream at catchment divide segments with elevations lower than those of blocking landslide tops. In this study, fluvial terraces and basal palaeovalley gravel beds were identified and differentiated from fan deltas (formed at tributary mouths entering dammed lakes). Application of selective geological and geomorphic criteria (summarized in Figure 1) enabled identification of seven diversion events and their effects in both coastal and inland settings of relatively small catchments. Evidence of river diversions is robust because it is supported as well by their geomorphic and sedimentary impacts in continental and submarine realms.

The landslides identified as causes of river diversion usually exhibit low-rupture surface dip and inconsequential internal brecciation. Most landslides exhibit still recognizable geomorphic and geological boundaries (main, minor and lateral scarps, toes and ridges), although they are masked by weathering, erosion, vegetation and profuse urbanization. Some of them can be considered large or giant attending to their current area. The positive correlation between landslide thicknesses (above their slip surfaces) and relief of the resultant dams permitted the latter to bear top elevations that led to overflow of dammed waters at catchment divide sites of lower elevation located upstream elsewhere. The maintenance of the internal coherence of the sliding mass contributes to the dam being thicker and higher. It is envisaged that their conjectured slow motion was occasionally accelerated (thus provoking river blocking) by combination of seismicity, storms and/or heavy rainfall and river incision.

ACKNOWLEDGEMENTS

We acknowledge the underground data availability made possible by the Town and City Councils of Aduna, Andoain, Donostia-San Sebastián, Errenteria, Ibarra, Lasarte-Oria, Oiartzun, Orio, Tolosa, Usurbil and Zarautz. We also thank access to geotechnical and hydrogeological reports facilitated by the Hydraulic Works and Roads Departments of Gipuzkoako Foru Aldundia, Euskal Trenbide Sarea-Red Ferroviaria Vasca, TPF Getinsa, Euroestudios, Esgemar S.A., Aquarium Donostia and Injelan S.A. Discussions and inputs provided over the years by several UPV/EHU colleagues, company geologists, etc. (L.M. Agirrezabala, A. da Silva, J.J. Esteban, B. Gascón, S. Luzuriaga, M. Ochoa, J.A. Pérez, J. Rodríguez, J.M. Sarasola, P. Tamés and A. Yangüas) are appreciated. We sincerely acknowledge the suggestions for improvement and comprehensive reviews provided by Laure Guerit and the journal associate editor Peter Burguess. Financial support came from the Euskal Herriko Unibertsitatea (GIU20/010).

CONFLICT OF INTEREST STATEMENT

There are no other conflicts of interest to declare.

PEER REVIEW

The peer review history for this article is available at https://www.webofscience.com/api/gateway/wos/peer-review/10.1111/bre.12798.

DATA AVAILABILITY STATEMENT

The data that support the findings of this study are available on request from the corresponding author.

ORCID

V. Iribar https://orcid.org/0000-0002-2353-3702
B. Ábalos https://orcid.org/0000-0003-4690-6468

REFERENCES

Ábalos, B. (2016). Geologic map of the Basque Cantabrian Basin and a new tectonic interpretation of the Basque arc. *International Journal of Earth Sciences*, *105*, 2327–2354. https://doi.org/10.1007/s00531-016-1291-6

Agliardi, F., Crosta, G. B., & Frattini, P. (2012). Slow rock-slope deformation. In J. J. Clague & D. Stead (Eds.), *Landslides: Types, mechanisms and modeling* (pp. 207–221). Cambridge University Press. https://doi.org/10.1017/CBO9780511740367.019

Altuna, J., Cearreta, A., Edeso, J. M., Elorza, M., Isturiz, M. J., Mariezkurrena, K., Mujika, J. A., & Ugarte, F. (1993). El yacimiento de Herriko-Barra (Zarautz, País Vasco) y su relación con las transgresiones marinas holocenas. In ITGME (Ed.), *El Cuaternario en España y Portugal* (Vol. *2*, pp. 923–942). Instituto Tecnológico GeoMinero de España.

Alvarez-Marrón, J., Hetzelb, R., Niedermannc, S., Menéndez, R., & Marquínez, J. (2008). Origin, structure and exposure history of a wave-cut platform more than 1 Ma in age at the coast of northern Spain: A multiple cosmogenic nuclide approach. *Geomorphology*, *93*, 316–334. https://doi.org/10.1016/j.geomorph.2007.03.005

Anton, L., Mather, A. E., Stokes, M., Muñoz-Martin, A., & De Vicente, G. (2015). Exceptional river gorge formation from unexceptional floods. *Nature Communications*, *6*, 7963. https://doi.org/10.1038/ncomms8963

AZTI. (2015). *Estudio morfo-sedimentario y geofísico de la bahía de La Concha de San Sebastián*. Donostiako Udala-Ayuntamiento de San Sebastián.

Barnolas, A., & Pujalte, V. (2004). La Cordillera Pirenaica: definición, límites y división. In J. A. Vera (Ed.), *Geología de España* (pp. 233–241). Sociedad Geológica de España – Instituto Geológico y Minero de España.

Benito-Calvo, A., Moreno, D., Fujioka, T., López, G. I., Martín-González, F., Martínez-Fernández, A., Hernando-Alonso, I., Karampaglidis, T., Bermúdez de Castro, J. M., & Francisco Gutiérrez, F. (2021). Towards the steady state? A long-term river incision deceleration pattern during pleistocene entrenchment (Upper Ebro River, Northern Spain). *Global and*

Planetary Change, *213*, 103813. https://doi.org/10.1016/j.gloplacha.2022.103813

Bhattacharya, J. P., Copeland, P., Lawton, T. F., & Holbrook, J. (2016). Estimation of source area, river paleo-discharge, paleoslope, and sediment budgets of linked deep-time depositional systems and implications for hydrocarbon potential. *Earth-Science Reviews*, *153*, 77–110. https://doi.org/10.1016/j.earscirev.2015.10.013

Bilbao-Lasa, P., Jara-Muñoz, J., Pedoja, K., Álvarez, I., Aranburu, A., Iriarte, E., & Galparsoro, I. (2020). Submerged marine terraces identification and an approach for numerical modeling the sequence formation in the Bay of Biscay (Northeastern Iberian Peninsula). *Frontiers in Earth Science*, *8*, 47. https://doi.org/10.3389/feart.2020.00047

Bishop, P. (1995). Drainage rearrangement by river capture, beheading and diversion. *Progress in Physical Geography*, *19*(4), 449–473. https://doi.org/10.1177/030913339501900402

Blum, M., Martin, J., Milliken, K., & Garvin, M. (2013). Paleovalley systems: Insights from Quaternary analogs and experiments. *Earth-Science Reviews*, *116*, 128–169. https://doi.org/10.1016/j.earscirev.2012.09.003

Bodego, A., & Agirrezabala, L. M. (2013). Syn-depositional thin- and thick-skinned extensional tectonics in the mid-Cretaceous Lasarte sub-basin, western Pyrenees. *Basin Research*, *25*, 594–612. https://doi.org/10.1111/bre.12017

Campos, J., & García-Dueñas, V. (1974). Mapa Geológico y Memoria de la Hoja n° 64 (San Sebastián). In *Mapa Geológico de España E. 1:50.000. Segunda Serie (MAGNA)* (Primera ed., p. 43). IGME.

Colman, S. M. (1983). Influence of the Onion Creek salt diapir on the late Cenozoic history of Fisher Valley, southeastern Utah. *Geology*, *11*, 240–243. https://doi.org/10.1130/0091-7613(1983)11

Costa, J. E., & Schuster, R. L. (1988). The formation and failure of natural dams. *GSA Bulletin*, *100*(7), 1054–1068. https://doi.org/10.1130/0016-7606(1988)100<1054:TFAFON>2.3.CO;2

Cuerpo de Ingenieros Militares. (1852). *Plano de la Plaza de San Sebastián y sus inmediaciones 1:10.000 scale — Plano n° 212 de la Cartoteca del Centro Geográfico del Ejército*.

Cuevas, J., Aranguren, A., Badillo, J. M., & Tubía, J. M. (1999). Estudio estructural del sector central del Arco Vasco (Cuenca Vasco-Cantábrica). *Boletín Geológico y Minero*, *110*, 3–18.

Dalrymple, R. W., Mackay, D. A., Ichaso, A. A., & Choi, K. S. (2012). Processes, morphodynamics, and facies of tide-dominated estuaries. In R. A. Davis, Jr. & R. W. Dalrymple (Eds.), *Principles of tidal sedimentology* (pp. 79–107). Springer. https://doi.org/10.1007/978-94-007-0123-6_5

Davis, W. M. (1890). The rivers and valleys of Pennsylvania. *National Geographic Magazine*, *1*, 183–253.

Davis, W. M. (1913). Meandering valleys and underfit rivers. *Annals of the Association of American Geographers*, *3*, 3–28.

DeFelipe, I., Pedreira, D., Pulgar, J. A., Beek, P. A., Bernet, M., & Pik, R. (2019). Unraveling the Mesozoic and Cenozoic tectonothermal evolution of the Eastern Basque-Cantabrian Zone–Western Pyrenees by low-temperature thermochronology. *Tectonics*, *38*, 3436–3461. https://doi.org/10.1029/2019TC005532

DeFelipe, I., Pulgar, J. A., & Pedreira, D. (2018). Crustal structure of the Eastern Basque-Cantabrian Zone-Western Pyrenees: From the Cretaceous hyperextension to the Cenozoic inversion. *Revista de la Sociedad Geológica de España*, *31*, 69–82.

del Val, M., Duvald, M., Medialdea, A., Bateman, M. D., Moreno, D., Arriolabengoa, M., Aranburu, A., & Iriarte, E. (2019). First chronostratigraphic framework of fluvial terrace systems in the eastern Cantabrian margin (Bay of Biscay, Spain). *Quaternary Geochronology*, *49*, 108–114. https://doi.org/10.1016/j.quageo.2018.07.001

del Val, M., Iriarte, E., Arriolabengoa, M., & Aranburu, A. (2015). An automated method to extract fluvial terraces from LIDAR based high resolution Digital Elevation Models: The Oiartzun valley, a case study in the Cantabrian Margin. *Quaternary International*, *364*, 35–43. https://doi.org/10.1016/j.quaint.2014.10.030

Delchiaro, M., Della Seta, M., Martino, S., Dehbozorgi, M., & Nozaem, R. (2019). Reconstruction of river valley evolution before and after the emplacement of the giant Seymareh rock avalanche (Zagros Mts., Iran). *Earth Surface Dynamics*, *7*, 929–947. https://doi.org/10.5194/esurf-7-929-2019

Demoulin, A., Bovy, B., Rixhon, G., & Cornet, Y. (2007). An automated method to extract fluvial terraces from digital elevation models: The Vesdre valley, a case study in eastern Belgium. *Geomorphology*, *91*, 51–64. https://doi.org/10.1016/j.geomorph.2007.01.020

Densmore, A. L., & Hovius, N. (2000). Topographic fingerprints of bedrock lanslides. *Geology*, *28*, 371–374.

DFG. (2006). *Nuevo proyecto de construcción de la variante de Orio en la carretera N-634*.

Discenza, M. E., & Esposito, C. (2021). State-of-art and remarks on some open questions about DSGSDs: Hints from a review of the scientific literature on related topics. *Italian Journal of Engineering Geology and Environment*, *1*, 31–59. https://doi.org/10.4408/IJEGE.2021-01.O-03

Douglass, J., Meek, M., Dorn, R. I., & Schmeeckle, M. W. (2009). A criteria-based methodology for determining the mechanism of transverse drainage development, with application to the southwestern United States. *GSA Bulletin*, *121*(3–4), 586–598. https://doi.org/10.1130/B26131.1

Dumont, T., Replumaz, A., Rouméjon, S., Briais, A., Rigo, A., & Bouillin, J.-P. (2015). Microseismicity of the Béarn range: Reactivation of inversion and collision structures at the northern edge of the Iberian plate. *Tectonics*, *34*, 934–950. https://doi.org/10.1002/2014TC003816

Dury, G. H. (1964). *Principles of underfit streams*. U.S. Geologic Survey, professional paper 452-A. U.S. Government Printing Office. https://doi.org/10.3133/PP452A

Eddey, L. J., Bateman, M. D., Livingstone, S. J., & Lee, J. R. (2022). New geomorphic evidence for a multi-stage proglacial lake associated with the former British–Irish Ice Sheet in the Vale of Pickering, Yorkshire, UK. *Journal of Quaternary Science*, *37*(8), 1407–1421. https://doi.org/10.1002/jqs.3413

Edeso, J. M. (2006). Caracterización granulométrica, morfométrica, litológica y sedimentológica de las terrazas fluviales del río Oiartzun (Gipuzkoa, País Vasco). *Lurralde: Investigación y Espacio*, *29*, 299–342. http://www.ingeba.org/lurralde/lurranet/lur29/edeso29/29edeso.htm

Edeso, J. M., Lopetegi, A., & Mujika, J. A. (2014). Quaternary Sea level changes in Jaizkibel: Sedimentary interpretation and geomorphological dynamics. *Munibe Monographs. Nature Series*, *2*, 25–46.

Edeso, J. M., Soria, A., Lopetegi, A., Mujika, J. A., & Ruiz, M. (2017). Estratigrafía y Sedimentología del relleno detrítico del estuario del Río Urumea (Donostia-San Sebastián, España). *Boletín de la Sociedad Geológica Mexicana*, *69*, 175–197.

ESGEMAR. (2015). *Estudio geofísico marino mediante sísmica de reflexión de alta resolución en la bahía de La Concha*. Donostiako Udala-Ayuntamiento de San Sebastián.

Euroestudios. (1971). *Proyecto de construcción Autopista Bilbao-Behobia*. Tramo IVc: Zarauz-S. Sebastian.

EVE. (1996). *Mapa Hidrogeológico del País Vasco* (p. 377). Ente Vasco de la Energía.

Fan, X., Dufresne, A., Siva Subramanian, S., Strom, A., Hermanns, A., Tacconi Stefanelli, C., Hewitt, K., Yunus, A. P., Dunningh, S., Capra, L., Geertsema, M., Miller, B., Casagli, N., Jansen, J. D., & Xu, Q. (2020). The formation and impact of landslide dams – State of the art. *Earth-Science Reviews*, *203*, 103116. https://doi.org/10.1016/j.earscirev.2020.103116

Flor, G., & Flor-Blanco, G. (2014). Raised beaches in the Cantabrian coast. In F. Gutiérrez & M. Gutiérrez (Eds.), *Landscapes and landforms of Spain*, world geomorphological landscapes (pp. 239–248). Springer. https://doi.org/10.1007/978-94-017-8628-7_20

Flor-Blanco, G., Flor, G. J., Morales, A., & Pando, L. (2015). Hydrodynamic controls of morpho-sedimentary evolution in a rockbounded mesotidal estuary. Tina Menor (N Spain). *Journal of Iberian Geology*, *41*, 315–332. https://doi.org/10.5209/rev_JIGE.2015.v41.n3.50313

Fryirs, K. A., & Brierley, G. J. (2013). *Geomorphic analysis of river systems: An approach to reading the landscape*. Wiley-Blacwell. https://doi.org/10.1002/9781118305454

Galparsoro, I., Borja, A., Legorburu, I., Hernández, C., Chust, G., Liria, P., & Uriarte, A. (2010). Morphological characteristics of the Basque continental shelf (Bay of Biscay, northern Spain); their implications for Integrated Coastal Zone Management. *Geomorphology*, *118*, 314–329. https://doi.org/10.1016/j.geomorph.2010.01.012

García, A. F. (2006). Thresholds of strath genesis deduced from landscape response to stream piracy by pancho Rico creek in the coast ranges of central California. *American Journal of Science*, *306*, 655–681. https://doi.org/10.2475/08.2006.03

Garcia-Castellanos, D. (2006). Long-term evolution of tectonic lakes: Climatic controls on the development of internally drained basins. *GSA Special Papers*, *398*, 283–294. https://doi.org/10.1130/2006.2398(17)

Garcia-Castellanos, D., & O'Connor, J. (2018). Outburst floods provide erodability estimates consistent with longterm landscape evolution. *Scientific Reports*, *8*(1), 10573. https://doi.org/10.1038/s41598-018-28981-y

Garrote, A., García, J., Muñoz, L., Fernández, J., Cerezo, A., Tijero, F., & Zapata, M. (1988). Mapa Geológico y Memoria de la Hoja n° 64-I (Zarautz). Mapa Geológico del País Vasco E. 1:25.000. EVE, 42 p.

Gibling, M. (2006). Width and thickness of fluvial channel bodies and valley fills in the geological record: A literature compilation and classification. *Journal of Sedimentary Research*, *76*, 731–770. https://doi.org/10.2110/jsr.2006.060

Gómez de Llarena, J. (1955). Terrazas fluviales. *Munibe. Sociedad de Ciencias Naturales Aranzadi (San Sebastian)*, *7*, 27–33.

Gómez, M., Vergés, J., & Riaza, C. (2002). Inversion tectonics of the northern margin of the Basque Cantabrian Basin. *Bulletin de la Société Géologique de France*, *173*, 449–459.

Guerit, L., Goren, L., Dominguez, S., Malavieille, J., & Castellfort, S. (2018). Landscape 'stress' and reorganization from χ-maps: Insights from experimental drainage networks in oblique collision setting. *Earth Surface Processes and Landforms*, *43*, 3152–3163. https://doi.org/10.1002/esp.4477

Gutiérrez, F., Sevil, J., Silva, P. G., Roca, E., & Escosa, F. (2019). Geomorphic and stratigraphic evidence of Quaternary diapiric activity enhanced by fluvial incision. Navarrés salt wall and graben system, SE Spain. *Geomorphology*, *342*, 176–195. https://doi.org/10.1016/j.geomorph.2019.06.002

Hancock, G. T., & Perrin, N. D. (2009). Green Lake Landslide and other giant and very large postglacial landslides in Fiordland, New Zealand. *Quaternary Science Reviews*, *28*, 1020–1036. https://doi.org/10.1016/j.quascirev.2008.08.017

Hanisch, J. (1974a). A "Sigsbee knoll" in early tertiary Bay of Biscay and associated turbidity currents. *American Association of Petroleum Geologists Bulletin*, *62*, 2232–2242. https://doi.org/10.1306/C1EA53C8-16C9-11D7-8645000102C1865D

Hanisch, J. (1974b). Der Tiefsee–Diapir von Zarauz (N–Spanien) im Spiegel von Sedimentation und Tektonik des Kreide/Tertiair–Flysches. *Geologisches Jahrbuch*, *B–11*, 101–142.

Hart, M. W., Shaller, P. J., & Farrand, G. T. (2012). When landslides are misinterpreted as faults: Case studies from the Western United States. *Environmental & Engineering Geoscience*, *18*, 313–325.

Hermanns, R. L., Folguera, A., Penna, I., Fauqué, L., & Niedermann, S. (2011). Landslide dams in the Central Andes of Argentina (Northern Patagonia and the Argentine Northwest). In S. G. Evans, R. L. Hermanns, A. L. Strom, & G. Scarascia Mugnozza (Eds.), *Natural and artificial rockslide dams, lecture notes in earth sciences* (Vol. *133*, pp. 147–176). Springer-Verlag. https://doi.org/10.1007/978-3-642-04764-0_5

Hermanns, R. L., Hewitt, K., Strom, A., Evans, S. G., Dunning, S. A., & Scarascia-Mugnozza, G. (2011). The classification of rockslide dams. In S. G. Evans, R. L. Hermanns, A. L. Strom, & G. Scarascia Mugnozza (Eds.), *Natural and artificial rockslide dams, lecture notes in earth sciences* (Vol. *133*, pp. 581–593). Springer-Verlag. https://doi.org/10.1007/978-3-642-04764-0_24

Hovius, N., Stark, C. P., & Allen, P. A. (1997). Sediment flux from a mountain belt derived by landslide mapping. *Geology*, *25*, 231–234.

Irabien, M. J., Cearreta, A., Gomez-Arozamena, J. G., & García-Artola, A. (2020). Holocene vs Anthropocene sedimentary records in a human-altered estuary: The Pasaia case (northern Spain). *Marine Geology*, *429*, 106292. https://doi.org/10.1016/j.margeo.2020.106292

Jaboyedoffa, M., Carreaa, D., Derrona, M.-H., Oppikoferb, T., Pennac, I. M., & Rudaza, B. (2020). A review of methods used to estimate initial landslide failure surface depths and volumes. *Engineering Geology*, *267*, 105478. https://doi.org/10.1016/j.enggeo.2020.105478

Johnson, K. N. (2016). *Causes and consequences of meandering in bedrock rivers: How interactions between rock properties and environmental conditions shape landscapes* (PhD thesis). UC Santa Cruz. https://escholarship.org/uc/item/812236pk

Johnson, K. N., & Finnegan, N. J. (2015). A lithologic control on active meandering in bedrock channels. *GSA Bulletin*, *127*(11/12), 1766–1776. https://doi.org/10.1130/B31184.1

Kennedy, D. M., & Paulik, R. (2007). Estuarine shore platforms in Whanganui Inlet, South Island, New Zealand. *Geomorphology*, *88*, 214–225. https://doi.org/10.1016/j.geomorph.2006.11.007

Korup, O. (2006). Landslide-induced river channel avulsions in mountain catchments of southwest New Zealand. *Geomorphology*, *63*, 57–80. https://doi.org/10.1016/j.geomorph.2004.03.005

Korup, O., Strom, A. L., & Weidinger, J. T. (2007). Fluvial response to large rock-slope failures: Examples from the Himalayas, the Tien Shan, and the Southern Alps in New Zealand. *Geomorphology*, *78*, 3–21. https://doi.org/10.1016/j.geomorph.2006.01.020

Lacroix, P., Handwergfer, A. L., & Bièvre, G. (2020). Life and death of slow-moving landslides. *Nature Reviews Earth & Environment*, *1*, 404–419. https://doi.org/10.1038/s43017-020-0072-8

Link, P. K., Crosby, B. T., Lifton, Z. M., Eversole, E. A., & Rittenour, T. M. (2014). The late Pleistocene (17 ka) Soldier Bar landslide and Big Creek Lake, Frank Church-River of No Return Wilderness, central Idaho, U.S.A. *Rocky Mountain Geology*, *49*(1), 17–31. https://doi.org/10.2113/gsrocky.49.1.17

Logan, R. L., & Schuster, R. L. (1991). Lakes divided: The origin of Lake Sutherland and Lake Crescent, Clallam County, Washington. *Washington Geology*, *19*(1), 38–42.

Loget, N., & Van Den Driessche, J. (2009). Wave train model for knickpoint migration. *Geomorphology*, *106*, 376–382. https://doi.org/10.1016/j.geomorph.2008.10.017

Ma, Q., Li, A., & Wang, P. (2023). Automatic detection of river capture based on planform pattern and χ-plot of the stream network. *Geomorphology*, *425*, 108587. https://doi.org/10.1016/j.geomorph.2023.108587

Mather, A., & Stokes, M. (2016). Extracting palaeoflood data from coarse-grained Pleistocene river terrace archives: An example from SE Spain. *Earth Surface Processes and Landforms*, *41*, 1991–2004. https://doi.org/10.1002/esp.4001

Mendicoa, J. (2011). The Holocene sedimentary infill of the Zarautz depression: Response to the eustatic sea-level rise. *Quaternary Studies*, *1*, 115–131.

Meunier, P., Hovius, N., & Haines, J. A. (2008). Topographic site effects and the location of earthquake induced landslides. *Earth and Planetary Science Letters*, *275*, 221–232.

Miall, A. D. (2014). *Fluvial depositional systems* (p. 316). Springer. https://doi.org/10.1007/978-3-319-00666-6

Monge-Ganuzas, M., Cearreta, A., Irabien, M. J., & García-Artola, A. (2019). Estuaries of the Basque coast. In J. A. Morales (Ed.), *The Spanish coastal systems* (pp. 437–465). Springer. https://doi.org/10.1007/978-3-319-93169-2_19

Nemec, W., & Steel, R. J. (1988). What is a fan delta and how do we recognize it? In W. Nemec & R. J. Steel (Eds.), *Fan deltas: Sedimentology and tectonic settings* (pp. 3–13). Blackie and Son.

OCSA. (2015). *Reconocimiento geofisico con sismica de refracción en la playa de Ondarreta (San Sebastián)*. Donostiako Udala-Ayuntamiento de San Sebastián.

Ouimet, W. B., Whipple, K. X., Crosby, B. T., Johnson, J. P., & Schildgen, T. F. (2008). Epigenetic gorges in fluvial landscapes. *Earth Surface Processes and Landforms*, *33*, 1993–2009. https://doi.org/10.1002/esp.1650

Pánek, T., & Klimeš, J. (2016). Temporal behavior of deep-seated gravitational slope deformations: A review. *Earth-Science Reviews*, *156*, 14–38. https://doi.org/10.1016/j.earscirev.2016.02.007

Pánek, T., Březný, M., Harrison, S., Schönfeldt, E., & Winocur, D. (2022). Large landslides cluster at the margin of a deglaciated mountain belt. *Scientific Reports*, *12*, 5658. https://doi.org/10.1038/s41598-022-09357-9

Pedrera, A., García-Senz, J., Ayala, C., Ruiz-Constán, A., Rodríguez-Fernandez, L. R., Robador, A., & González-Menéndez, L. (2017). Reconstruction of the exhumed mantle across the north Iberian margin by crustal-scale 3-D gravity inversion and geological cross section. *Tectonics*, *36*, 3155–3177. https://doi.org/10.1002/2017TC004716

Pedrera, A., García-Senz, J., Peropadre, C., Robador, A., López-Mir, B., Díaz-Alvarado, J., & Rodríguez-Fernandez, L. R. (2021). The Getxo crustal-scale cross section: Testing tectonic models in the Bay of Biscay-Pyrenean rift system. *Earth-Science Reviews*, *221*, 103429. https://doi.org/10.1016/j.earscirev.2020.103429

Retallack, G. J., & Roering, J. J. (2012). Wave-cut or water-table platforms of rocky coasts and rivers? *GSA Today*, *22*(6), 4–10. https://doi.org/10.1130/GSATG144A.1

Ríos, J. M. (1948). Diapirismo. *Boletín del Instituto Geológico y Minero de España*, *60*, 155–390.

Ruiz, M., Gallart, J., Díaz, J., Olivera, C., Pedreira, D., López, C., González-Cortina, J. M., & Pulgar, J. A. (2006). Seismic activity at the western Pyrenean edge. *Tectonophysics*, *412*(217), 235. https://doi.org/10.1016/j.tecto.2005.10.034

Santana, R. (1966a). *Géomorphologie des bassins de la Bidasoa et de l'Urumea* (Thèse de doctorat d'université). Institut de Géographie, Faculté des Lettres et Sciences Humaines, 1–162.

Santana, R. (1966b). Evolución Geomorfológica del litoral Guipuzcoano. País Vasco Español. In *Estudios geográficos: Homenaje de la Facultad de Filosofia y Educación a don Humberto Fuenzalida Villegas* (pp. 165–184). Facultad de Filosofía y Educación, Universidad de Chile.

Sklar, L. S., & Dietrich, W. E. (2006). The role of sediment in controlling steady-state bedrock channel slope: Implications of the saltation-abrasion incision model. *Geomorphology*, *82*, 58–83. https://doi.org/10.1016/j.geomorph.2005.08.019

Spratt, R. M., & Lisiecki, L. E. (2016). A Late Pleistocene sea level stack. *Climate of the Past*, *12*, 1079–1092. https://doi.org/10.5194/cp-12-1079-2016

Stead, D., & Wolter, A. (2015). A critical review of rock slope failure mechanisms: The importance of structural geology. *Journal of Structural Geology*, *74*, 1–23. https://doi.org/10.1016/j.jsg.2015.02.002

Teixell, A., Labaume, P., Ayarza, P., Espurt, N., de Saint Blanquat, M., & Lagabrielle, Y. (2018). Crustal structure and evolution of the Pyrenean-Cantabrian belt: A review and new interpretations from recent concepts and data. *Tectonophysics*, *734-735*, 130–147. https://doi.org/10.1016/j.tecto.2018.04.017

Tofiño de San Miguel, V. (1788). *Atlas marítimo de España*. Retrieved July 28, 2016, from http://www.cervantesvirtual.com/obra/atlas-maritimo-de-espana/

Twidale, C. R. (2004). River patterns and their meaning. *Earth-Science Reviews*, *67*, 159–218. https://doi.org/10.1016/j.earscirev.2004.03.001

Valdés, J. M. (1942). Informe de la Jefatura de sondeos y estudio geológicos. In J. M. Aguirre (Ed.), *Memoria que manifiesta el progreso y desarrollo del Puerto de Pasajes desde su reversión al Estado en enero de 1927 hasta diciembre de 1941* (pp. 194–198). Talleres Gráficos Laborde y Labayen.

Wang, R., Colombera, L., & Mountney, N. P. (2019). Geological controls on the geometry of incised-valley fills: Insights from a global dataset of late-quaternary examples. *Sedimentology*, *66*, 2134–2168. https://doi.org/10.1111/sed.12596

Willett, S. D., McCoy, S. W., Perron, J. T., Goren, L., & Chen, C.-Y. (2014). Dynamic reorganization of river basins. *Science*, *343*, 1248765. https://doi.org/10.1126/science.1248765

Zabaleta, A., Antigüedad, I., Barrio, I., & Probst, J. L. (2016). Suspended sediment delivery from small catchments to the Bay of Biscay. What are the controlling factors? *Earth*

Surface Processes and Landforms, *41*, 1894–1910. https://doi.org/10.1002/esp.3957

Zhang, X., Wang, S., Wu, X., Xu, S., & Li, Z. (2016). The development of a laterally confined laboratory fan delta under sediment supply reduction. *Geomorphology*, *257*, 120–133. https://doi.org/10.1016/j.geomorph.2015.12.027

Zhang, Y., Dai, X., Wang, M., & Li, X. (2020). The concept, characteristics and significance of fluvial fans. *Petroleum Exploration and Development*, *47*, 1014–1026. https://doi.org/10.1016/S1876-3804(20)60113-6

Zhonga, Q., Chena, S., & Shana, Y. (2020). Prediction of the overtopping-induced breach process of the landslide dam. *Engineering Geology*, *274*, 105709. https://doi.org/10.1016/j.enggeo.2020.105709

How to cite this article: Iribar, V., & Ábalos, B. (2023). Pleistocene river diversions caused by large landslides in the western Pyrenees (Oria River drainage basin, N Spain). *Basin Research*, *35*, 2268–2300. https://doi.org/10.1111/bre.12798